

---

# A mathematical model of granulopoiesis incorporating the negative feedback dynamics and kinetics of G-CSF/neutrophil binding and internalisation

M. Craig · A.R. Humphries ·  
M.C. Mackey

the date of receipt and acceptance should be inserted later

**Abstract** We develop a physiological model of granulopoiesis which includes explicit modelling of the kinetics of the cytokine granulocyte colony-stimulating factor (G-CSF) incorporating both the freely circulating concentration and the concentration of the cytokine bound to mature neutrophils. G-CSF concentrations are used to directly regulate neutrophil production, with the rate of differentiation of stem cells to neutrophil precursors, the effective proliferation rate in mitosis, the maturation time, and the release rate from the mature marrow reservoir into circulation all dependent on the level of G-CSF in the system. The dependence of the maturation time on the cytokine concentration introduces a state-dependent delay into our differential equation model, and we show how this is derived from an age-structured partial differential equation model of the mitosis and maturation, and also detail the derivation of the rest of our model. The model and its estimated parameters are shown to successfully predict the neutrophil and G-CSF responses to a variety of treatment scenarios, including the combined administration of chemotherapy and exogenous G-CSF. This concomitant treatment was reproduced *without any additional fitting* to characterise drug-drug interactions.

---

M. Craig  
Faculté de Pharmacie, Université de Montréal, Montréal, QC, Canada H3T 1J4  
E-mail: morgan.craig@umontreal.ca

A.R. Humphries  
Department of Mathematics and Statistics, McGill University, Montréal, QC, Canada, H3A 0B9  
E-mail: tony.humphries@mcgill.ca

M.C. Mackey  
Departments of Mathematics, Physics and Physiology, McGill University, Montréal, QC, Canada, H3G 1Y6  
E-mail: michael.mackey@mcgill.ca

**Keywords** Granulopoiesis · mathematical modelling · state-dependent delay differential equations · physiologically constructed pharmacokinetics · G-CSF · bound and unbound drug concentrations

## 1 Introduction

We present a new model of granulopoiesis, in which the production of neutrophils is governed by a negative feedback loop between the neutrophils and granulocyte colony stimulating factor (G-CSF). G-CSF is the principal cytokine known to regulate neutrophil production and in our model it is used to moderate differentiation of stem cells, apoptosis of proliferating neutrophil precursors, the speed at which neutrophils mature and the rate that mature neutrophils are released from the marrow reservoir. To facilitate this, we derive not only new functions for the pharmacodynamic effects of G-CSF, but also a new model of the G-CSF kinetics which incorporates cytokine binding and internalisation by the neutrophils. We dispense with the mass action law assumption made in some previous models and directly model the concentration of both circulating G-CSF and G-CSF bound to neutrophils. This improved kinetic model furnishes us with G-CSF concentrations which are considerably more accurate than our previous models so we are able to use them to directly drive the pharmacodynamic effects and finally form a fully closed cytokine-neutrophil feedback loop.

At homeostasis the dominant removal mechanism for G-CSF is internalisation by neutrophils after it binds to receptors on these cells [32]. This gives rise to a negative feedback mechanism on the G-CSF pharmacokinetics (PKs) whereby large concentrations of neutrophils result in G-CSF being removed from circulation, in turn leading to low concentrations of circulating G-CSF. On the other hand if neutrophil concentrations are reduced then G-CSF is not cleared from circulation as quickly and circulating concentrations increase as a result. The feedback loop is completed by the pharmacodynamic (PD) effects of the G-CSF: elevated (depressed) G-CSF levels lead to increased (decreased) neutrophil production. Due to this feedback, using the simple paradigm that neutrophil concentration is a cipher for the cytokine concentration (with one low when the other is high), it is possible to derive granulopoiesis models without explicitly modelling the cytokines. This is particularly useful because it is not universally agreed where or how the multitude of identified cytokines all act.

The mathematical modelling of granulopoiesis has a long and rich history [4, 5, 9, 11, 18, 20, 25, 27, 28, 53, 54, 56, 57, 61, 72, 65, 66, 68] but one of the earliest and most complete treatments is that of Rubinow [49] which incorporates a number of features that we retain in our model, including active proliferation, maturation, a marrow reservoir and free exchange between the circulating and marginal blood neutrophil pools. Rubinow's model, however, predates the discovery and characterisation of G-CSF and so it uses neutrophil concentrations as a cipher for the cytokine and its effects. Subsequent physiological models

have also all incorporated at least some elements of this cytokine paradigm in their modelling. Some authors have been principally interested in neutrophil pathologies, including cyclical neutropenia, chronic myeloid leukemia, and myelosuppression during chemotherapy, while others have primarily studied the effects of G-CSF mimetics. Many models of cyclic neutropenia, including [9, 18, 25, 33] and [55] acknowledge the role of G-CSF in neutrophil production and pathologies but rely on the cytokine paradigm to drive the pharmacodynamic responses. A number of modelling approaches have been proposed, including compartmental ODE models [53, 21, 46, 22, 30, 69], delay differential equations (DDEs) incorporating statistical distributions to model delays [66, 65], and DDEs derived from age-structured partial differential equation (PDE) models, like the one developed in this work [5, 11, 20].

In recent years, synthetic forms of G-CSF have been developed and are administered to patients for a variety of reasons, including to treat cyclical neutropenia or as an adjuvant during chemotherapy [12, 13, 40]. However, the administration of exogenous G-CSF breaks the cytokine paradigm and it is possible for neutrophil and G-CSF concentrations to both be elevated at the same time. This breakdown of the natural feedback relationship can cause physiological models that use the paradigm to mischaracterise the elimination dynamics of G-CSF. For example, both [30] and [11] overestimate the renal clearance of G-CSF so much as to essentially eliminate the contribution of neutrophil-mediated internalisation, even though they each include this non-linear clearance in their models. If elevated neutrophil concentrations are used to drive the system dynamics on the assumption that corresponding G-CSF concentrations are reduced when they are in fact elevated, the modelled effects will act in the opposite sense to the physiology. As a consequence, the model will either develop instabilities and/or give a poor fit to observed dynamics.

The mischaracterisation of G-CSF elimination dynamics was the impetus for the current work. Consequently, we will not use the neutrophil concentration as a cipher for the G-CSF concentration, but will model both the G-CSF pharmacokinetics and pharmacodynamics (PK/PD) in detail. For this, we develop a novel pharmacokinetic model of G-CSF which includes both unbound and bound blood concentrations. The G-CSF concentrations given by this kinetic model are then used to drive the pharmacodynamic effects of the cytokine, in a fully formed negative feedback loop.

We begin by summarising the granulopoiesis model in Section 2. Its development is then extensively detailed in Section 3, beginning from the stem cells in Section 3.1. The novel pharmacokinetic G-CSF model incorporating bound and unbound blood concentrations is motivated and developed in Section 3.2. There we show how the hypothesis of an equilibrium between bound and unbound concentrations is not satisfied for G-CSF, necessitating the inclusion of more complex kinetics in its pharmacokinetic model. Next, the derivation of the DDE granulopoiesis model is given in Section 3.3 and the pharmacodynamic model of G-CSF is developed in Section 3.4. Models of the exogenous drugs considered in our study are detailed in Section 3.5. Having laid the foundations of our model, the various methods of parameter estimation and

fitting used for our analyses are subsequently explained in Section 4. These approaches include model-specific constraints, as seen in Sections 4.1 and 4.3, while fitting procedures from published data are described in Sections 4.2, 4.4, and 4.5. The resulting parameters are then summarized in Section 5. Finally in Section 6 we put our model to the acid test of *predicting (not fitting)* the population neutrophil response in a group of patients undergoing simultaneous chemotherapy and G-CSF administration [42, 43] and obtain excellent agreement between the model predicted behavior and the clinical data. We conclude with a short discussion in Section 7.

## 2 Model Summary

Here we define the variables and summarise the equations that define our granulopoiesis model. A detailed derivation is contained in Section 3. Figure 1 shows a schematic diagram describing the main elements of the hematopoietic system that we model.

The hematopoietic stem cell (HSC), neutrophil and G-CSF model is a set of five differential equations including constant and state-dependent delays. Let  $Q(t)$  be the concentration of HSCs at time  $t$ ,  $N_R(t)$  be the concentration of mature neutrophils in the marrow reservoir, and  $N(t)$  be the concentration of the total blood neutrophil pool (TBNP) at time  $t$  (which includes both circulating and marginated neutrophils). Further, let  $G_1(t)$  be the concentration of unbound, circulating G-CSF and  $G_2(t)$  be the concentration of G-CSF bound to receptors on mature neutrophils (in the reservoir or in the blood neutrophil pool).

The production of neutrophils from the HSCs is modelled by

$$\begin{aligned} \frac{d}{dt}Q(t) = & -(\kappa(G_1(t)) + \kappa_\delta + \beta(Q(t)))Q(t) \\ & + A_Q(t)\beta(Q(t - \tau_Q))Q(t - \tau_Q) \end{aligned} \quad (1)$$

$$\begin{aligned} \frac{d}{dt}N_R(t) = & A_N(t)\kappa(G_1(t - \tau_N(t)))Q(t - \tau_N(t))\frac{V_{N_M}(G_1(t))}{V_{N_M}(G_1(t - \tau_{N_M}(t)))} \\ & - (\gamma_{N_R} + \varphi_{N_R}(G_1(t)))N_R(t) \end{aligned} \quad (2)$$

$$\frac{d}{dt}N(t) = \varphi_{N_R}(G_{BF}(t))N_R(t) - \gamma_N N(t), \quad (3)$$

with the concentrations of G-CSF (unbound and bound to neutrophil G-CSF receptors) given by

$$\begin{aligned} \frac{d}{dt}G_1(t) = & I_G(t) + G_{prod} - k_{ren}G_1(t) \\ & - k_{12}([N_R(t) + N(t)]V - G_2(t))G_1(t)^{Pow} + k_{21}G_2(t) \end{aligned} \quad (4)$$

$$\frac{d}{dt}G_2(t) = -k_{int}G_2(t) + k_{12}([N_R(t) + N(t)]V - G_2(t))G_1(t)^{Pow} - k_{21}G_2(t), \quad (5)$$

where  $I_G(t)$  indicates input of exogenous G-CSF, which we assume is filgrastim (the most common bio-similar exogenous form of G-CSF). Filgrastim has very similar PK/PD properties to endogenous G-CSF, so we will not distinguish between the two types of G-CSF in our model.

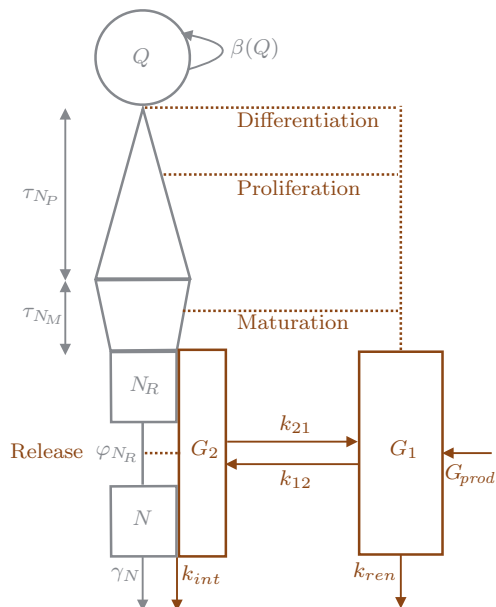


Fig. 1: Schematic representation of the production of circulating neutrophils in the bone marrow and the interaction of the system with G-CSF. Hematopoietic stem cells (HSCs- $Q$ ) enter the neutrophil lineage, the other blood lines, or are removed from the HSC pool. Differentiated HSCs then undergo successive divisions during the proliferative phase. Cells then mature before being stored in the marrow reservoir, or dying off during maturation. Neutrophils remain in the reservoir until they are removed randomly or enter the circulation, where they disappear rapidly from the blood. Freely circulating G-CSF may bind to receptors on the neutrophils. The concentration of bound G-CSF drives its pharmacodynamic effects. The concentration of G-CSF bound to mature neutrophils,  $G_2$ , determines the rate of release from the marrow reservoir. The concentration of G-CSF bound to neutrophil precursors, assumed proportional to  $G_1$  the concentration of freely circulating G-CSF, determines the rate of differentiation from the HSCs, the speed of maturation, and the rate of proliferation. For all four effects, speed and rates increase with increasing G-CSF concentration.

The derivation of these equations is given in Section 3. In Section 3.3, particular attention is paid to the derivation of the state-dependent delay terms in (2) from an age-structured partial differential equation (PDE) model of the mitosis and maturation with variable aging rate of the neutrophil precursors. The G-CSF equations (4),(5) are explained in detail in Section 3.2.

In the stem cell equation (1), as explained in Section 3.1, we have

$$\beta(Q) = f_Q \frac{\theta_2^{s_2}}{\theta_2^{s_2} + Q^{s_2}}, \quad (6)$$

$$A_Q(t) = A_Q^* = 2e^{-\gamma_Q \tau_Q}. \quad (7)$$

Only in the case of administration of chemotherapy is the stem cell amplification factor  $A_Q(t)$  non-constant. During chemotherapeutic treatment  $A_Q(t)$  will be modified by replacing (7) with (38) as discussed in Section 3.5. Stem cells commit to differentiate to neutrophil precursors at a rate given by

$$\kappa(G_1) = \kappa^* + (\kappa^* - \kappa^{min}) \left[ \frac{G_1^{s_1} - (G_1^*)^{s_1}}{G_1^{s_1} + (G_1^*)^{s_1}} \right]. \quad (8)$$

Here, and throughout, the superscript  $*$  denotes the homeostasis value of a quantity. The rationale for using (8) to describe the pharmacodynamic effect of the G-CSF on the differentiation of the HSCs, along with the other  $G_1$ -dependent functions is explained in Section 3.4.

After entering the neutrophil lineage, cells undergo mitosis at a variable rate ( $\eta_{N_P}(G_1(t))$ ) given by

$$\eta_{N_P}(G_1(t)) = \eta_{N_P}^* + (\eta_{N_P}^* - \eta_{N_P}^{min}) \frac{b_{N_P}}{G_1^*} \left( \frac{G_1(t) - G_1^*}{G_1(t) + b_{N_P}} \right) \quad (9)$$

for a proliferation time  $\tau_{N_P}$ , considered to be constant. Cells subsequently mature at a variable aging rate given by

$$V_{N_M}(G_1(t)) = 1 + (V_{max} - 1) \frac{G_1(t) - G_1^*}{G_1(t) - G_1^* + b_V}, \quad (10)$$

until they reach age  $a_{N_M}$  so the time  $\tau_{N_M}(t)$  it takes for a neutrophil maturing at time  $t$  to mature satisfies the integral relationship

$$\int_{t-\tau_{N_M}(t)}^t V_{N_M}(G_1(s)) ds = a_{N_M}. \quad (11)$$

At homeostasis,  $V_{N_M}(G_1^*) = 1$ , and thus  $a_{N_M}$  is the homeostatic maturation time. The total time it takes a neutrophil to be produced (from HSC differentiation to release into the reservoir pool) is

$$\tau_N(t) = \tau_{N_P} + \tau_{N_M}(t), \quad (12)$$

and we can differentiate equation (11) to obtain the following DDE for both  $\tau_N$  and  $\tau_{N_M}$

$$\frac{d}{dt} \tau_N(t) = \frac{d}{dt} \tau_{N_M}(t) = 1 - \frac{V_{N_M}(G_1(t))}{V_{N_M}(G_1(t - \tau_{N_M}(t)))}. \quad (13)$$

Maturing neutrophils are assumed to die at a constant rate given by  $\gamma_{N_M}$ . The amplification factor  $A_N(t)$  between differentiation from HSCs to maturation that appears in (2) is then given by

$$A_N(t) = \exp \left[ \int_{t-\tau_N(t)}^{t-\tau_{N_M}(t)} \eta_{N_P}(G_1(s)) ds - \gamma_{N_M} \tau_{N_M}(t) \right] \quad (14)$$

as derived in Section 3.3. Numerical implementation of the neutrophil amplification rate is obtained by differentiating the integral expressions in (14) using Leibniz's Rule to obtain

$$\begin{aligned} \frac{d}{dt} A_N(t) = A_N(t) & \left[ \left(1 - \frac{d}{dt} \tau_{N_M}(t)\right) (\eta_{N_P}(G_1(t-\tau_{N_M}(t))) - \eta_{N_P}(G_1(t-\tau_N(t)))) \right. \\ & \left. - \gamma_{N_M} \frac{d}{dt} \tau_{N_M}(t) \right]. \quad (15) \end{aligned}$$

After maturation neutrophils are sequestered into the marrow neutrophil reservoir. Mature neutrophils exit the reservoir either by dying with constant rate  $\gamma_{N_R}$ , or by being released into circulation with a rate  $\varphi_{N_R}$  depending on the fraction  $G_{BF}(t)$  of neutrophil receptors that are bound by G-CSF. We define

$$G_{BF}(t) = \frac{G_2(t)}{V[N_R(t) + N(t)]} \in [0, 1], \quad G_{BF}^* = \frac{G_2^*}{V[N_R^* + N^*]}, \quad (16)$$

and let

$$\varphi_{N_R}(G_{BF}(t)) = \varphi_{N_R}^* + (\varphi_{N_R}^{max} - \varphi_{N_R}^*) \frac{G_{BF}(t) - G_{BF}^*}{G_{BF}(t) - G_{BF}^* + b_G}. \quad (17)$$

Neutrophils are removed from circulation with constant rate  $\gamma_N$ .

In equations (1)–(5) we use units of  $10^9$  cells per kilogram (of body mass) for the reservoir and circulating neutrophils, and  $10^6$  cell/kg for the stem cells. The scaling factors ensure that computations are performed with numbers of similar magnitude which improves numerical stability. Circulating and bound G-CSF concentrations are measured in standard units of nanograms per millilitre of blood. The differing units for neutrophils and G-CSF are only problematic in equations (4), (5) where quantities in both units appear; see Section 4.2 for the derivation of the conversion factor  $V$ .

Its also important to note that  $N(t)$  measures the total blood neutrophil pool, including both the circulating and marginated neutrophils. To convert  $N(t)$  to an absolute neutrophil count/circulating neutrophil numbers  $N_C(t)$  (or *vice versa*) there is a conversion factor; see (93).

### 3 Model Development

Here we describe the development of our granulopoiesis model leading to the equations presented in Section 2. The equation for the stem cells (1) is described briefly in Section 3.1. The size of the mature neutrophil reservoir is

described by (2). The first term on the right-hand side of this equation gives the rate that mature neutrophils enter the reservoir. This term is derived from an age-structured PDE model described in Section 3.3 below. Neutrophils are assumed to leave the reservoir either by dying at rate  $\gamma_{N_R}$  or by entering into circulation at rate  $\varphi_{N_R}$ , and are removed from circulation at a constant rate  $\gamma_N$ . In Section 3.2 we describe our new G-CSF model (4),(5) of the unbound freely circulating G-CSF ( $G_1$ ), and the G-CSF bound to receptors on the neutrophils ( $G_2$ ). This model allows us to model the pharmacodynamic effects of the G-CSF directly as detailed in Section 3.4. Finally, Section 3.5 outlines our models for the exogenous drugs we will consider in later sections.

### 3.1 Stem Cells

Equation (1) for the stem cell dynamics was previously used in [35,8,9,45,20,33,5,11]. In particular, see [4] for a detailed derivation. Here, we remove the dependence of  $\gamma_Q$  upon G-CSF as the HSC population is relatively stable and infrequently dividing [48,16] and, to our knowledge, no direct evidence of G-CSF's action upon HSC apoptosis currently exists. Craig [11] uses

$$A_Q(t) = 2 \exp \left[ - \int_{t-\tau_Q}^t \gamma_Q(s) ds \right], \quad (18)$$

and in the absence of chemotherapy we take the apoptotic rate  $\gamma_Q$  to be constant so this becomes (7).

### 3.2 A physiologically constructed pharmacokinetic G-CSF model

A new pharmacokinetic model of G-CSF, already stated in (4),(5) is used to model the concentrations of both unbound and bound G-CSF. We do not distinguish between endogenous and exogenous G-CSF in the model, which constrains us to only consider biosimilar forms of exogenous G-CSF. Accordingly, we focus on filgrastim, the most widely-available form of exogenous G-CSF. However, other less common forms of biosimilar exogenous G-CSF are available and include lenograstim and Nartograstim<sup>®</sup> [40]. The pegylated form of rhG-CSF has greatly reduced renal clearance relative to endogenous G-CSF, which would require a different model, so we will not consider it in this work.

In equations (4),(5)  $G_1$  is the concentration of freely circulating G-CSF and  $G_2$  is the concentration of G-CSF which is bound to receptors on the neutrophils. Since the bone marrow is well perfused, G-CSF can bind to mature neutrophils in the marrow reservoir as well as neutrophils in circulation. In the model  $k_{ren}$  denotes the nonsaturable removal rate of circulating G-CSF (mainly renal).  $k_{int}$  denotes the removal rate of bound-G-CSF, which we refer to as the effective internalisation rate. This term models the removal of bound G-CSF both by internalisation after binding and through the removal of the neutrophil itself from circulation (along with its bound G-CSF molecules).



$k_{12}$  is the rate of binding of free G-CSF to the neutrophils, and  $Pow$  is the effective binding coefficient. The G-CSF receptor has a 2:2 stoichiometry in *in vitro* studies [32], so a simple chemical reaction model would suggest  $Pow = 2$ . However, the number of ligands binding to a receptor only provides an upper bound on the corresponding Hill coefficient [51]. Accordingly, we use an effective binding coefficient  $Pow \in [1, 2]$ .

In this model the bound G-CSF concentration is saturable, with  $V[N_R(t) + N(t)]$  being the capacity of this compartment.  $G_2 = V[N_R(t) + N(t)]$  would indicate that every receptor on every neutrophil in the reservoir and circulation was bound to two G-CSF molecules. Thus the removal rate of neutrophils by internalisation is saturable. G-CSF also binds to immature neutrophils and precursors, which will be important for the pharmacodynamics, but since these cells are fewer in number and/or have fewer receptors than the mature neutrophils we neglect this effect on the pharmacokinetics. Finally,  $k_{21}$  is the rate of unbinding (transformation from bound G-CSF to circulating G-CSF), and  $I_G(t)$  denotes exogenous administration of G-CSF, discussed in Section 3.5.

If we were to assume that there is no net transfer between the bound and circulating G-CSF then letting  $\tilde{N}(t) = [N_R(t) + N(t)]$ , equations (4),(5) imply

$$k_{12}(V\tilde{N}(t) - G_2)G_1^{Pow} - k_{21}G_2 \approx 0. \quad (19)$$

Rearranging (19) we obtain

$$G_2(t) \approx \frac{[G_1(t)]^{Pow}}{[G_1(t)]^{Pow} + k_{21}/k_{12}} V\tilde{N}(t).$$

Now, adding (4) and (5)

$$\frac{d}{dt}(G_1 + G_2) \approx I_G(t) + G_{prod} - k_{ren}G_1 - k_{int}G_2,$$

and assuming that  $G_1 \gg G_2$  and that  $\frac{d}{dt}(G_1 + G_2) \approx \frac{d}{dt}G_1$ , and finally replacing the  $\approx$  by an equality we have

$$\frac{d}{dt}G_1 = I_G(t) + G_{prod} - k_{ren}G_1 - k_{int}V\tilde{N}(t)\frac{[G_1(t)]^{Pow}}{[G_1(t)]^{Pow} + k_{21}/k_{12}}. \quad (20)$$

Equations similar to (20) have been used to model G-CSF pharmacokinetics in many papers including [11, 5, 20, 30, 29, 69], but usually with  $\tilde{N}(t) = N(t)$  the concentration of circulating neutrophils, as opposed to  $\tilde{N}(t) = [N_R(t) + N(t)]$  as (4),(5) suggest.

The usual derivation of (20) is from the law of mass action, but this is equivalent to the assumption (19) that the bound and circulating G-CSF are in quasi-equilibrium. However, the equilibrium hypothesis (19) cannot hold at homeostasis, since if (19) holds and  $k_{int} > 0$  then  $\frac{d}{dt}G_2 < 0$  which is contradictory. Clinical evidence [52, 64] suggests that at homeostasis, binding and internalisation is the dominant removal mechanism for G-CSF, so not only does (19) not hold but the net transfer from unbound to bound G-CSF should be more than  $0.5 \times G_{prod}$ . Another important situation where (19) will fail is

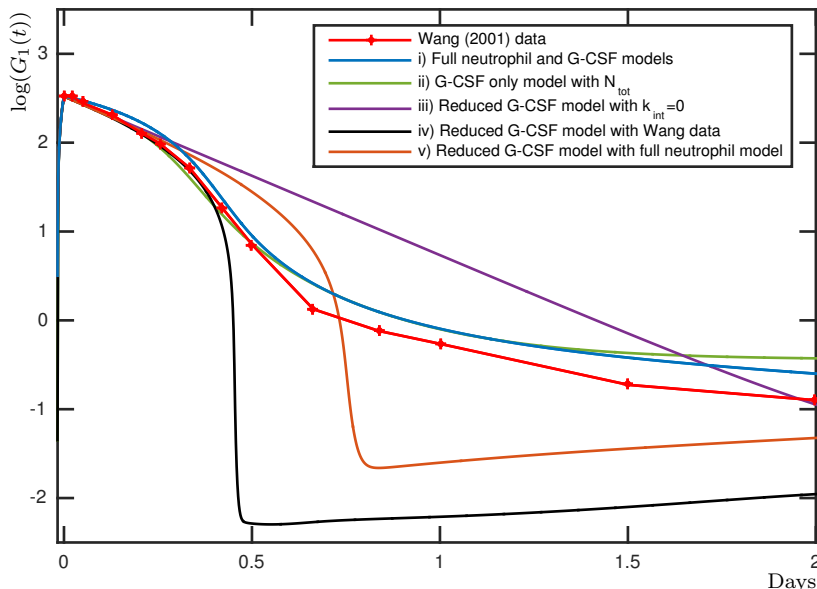


Fig. 2: Data from Wang [69] for G-CSF concentrations after a  $750 \mu\text{g}$  25 minute IV infusion and five different simulations: (i) the full neutrophil and G-CSF model (1)–(5) (ii) the G-CSF only model (68),(69), (iii) the reduced G-CSF model (20) with  $k_{int} = 0$ , (iv) the reduced G-CSF model (20) with  $k_{int} = 30$  and  $\tilde{N}(t) = N(t)$  and neutrophil concentrations taken from the Wang [69] and (v) the full neutrophil model (1)–(3) and the reduced G-CSF model (20) with  $k_{int} = 25$  and  $\tilde{N}(t) = [N_R(t) + N(t)]$ . In ii)  $N_{tot} = 4.1457$  and  $G_2^*$  and  $G_{prod}$  are determined by Equations (74) and (76), respectively. In (ii), (iv) and (v)  $k_{ren} = 4.12$  and  $G_{prod}$  is determined by (20). All other parameters take values specified in the third columns of Tables 1 and 2.

during exogenous administration of G-CSF, which will initially increase the concentration of unbound G-CSF (often by orders of magnitude).

Figure 2 illustrates some of the issues involved in modelling the kinetics of G-CSF. This figure shows data from a  $750 \mu\text{g}$  intravenous (IV) infusion digitised from Figure 6 of Wang [69], along with a number of simulations of the protocol using different G-CSF kinetic models. The data in Figure 2 seems to have at least two different slopes, suggesting that the G-CSF time course could be approximated by the sum of two exponentials. This naturally leads to two compartment pharmacokinetic models [15]. Such a two-compartment G-CSF model was previously considered by Kuwabara [31] for Nartograstim<sup>®</sup>. Consistent with general two-compartment models in pharmacology, the two compartments corresponded to the blood and the tissues, and generic saturable and nonsaturable removal of the G-CSF both occurred from the blood compartment. This differs from our model where elimination occurs from the

two compartments (which instead represent unbound and bound G-CSF concentrations), both of which are subject to linear elimination. By contrast, in our model one compartment is saturable with nonsaturable elimination (the bound G-CSF), which corresponds to known G-CSF removal mechanisms. The assignment of elimination to the first or second compartments also has significant effects on the estimation of corresponding pharmacokinetic parameters so the mischaracterisation of these elimination dynamics could have significant effects on the model's predictions and behaviours [73].

The circulating G-CSF concentration time course for a simulation of our full model (1)–(5) tracks the measured G-CSF data very closely in Figure 2. It slightly overestimates the G-CSF, but it is important to note that the data points are average values from a number of subjects and we will see in Section 4.2 that our G-CSF concentrations are well within the data range for several of administration protocols.

Also shown in Figure 2 is a simulation of a simplified version of the G-CSF equations (4),(5) where the time dependent neutrophil term  $[N_R(t) + N(t)]$  is replaced by a constant  $N_{tot}$ , so the G-CSF kinetic equations become independent of the neutrophil dynamics. The resulting equations are stated as (68),(69) in Section 4.2 where they are used to determine the pharmacokinetic parameters that appear in (4),(5). The constant  $N_{tot}$  can be thought of as a time average of the term  $[N_R(t) + N(t)]$ . As seen in Figure 2, this stand-alone simplified G-CSF model gives G-CSF concentrations very close to those of the full model, which justifies using it to determine the kinetic parameters.

Three different simulations of the single G-CSF equation (20) are also shown in Figure 2 to illustrate the difficulties in dealing with reduced models. One simulation has  $k_{int} = 0$  so that the elimination of G-CSF is purely renal and it is clear that the nuances of the G-CSF kinetics are lost.

A simulation of (20) with  $k_{int} > 0$  and  $\tilde{N}(t) = N(t)$  (with values for  $N(t)$  taken from the Wang data) gives even worse results than the purely renal elimination case. The problem with this model is that for the first few hours while the neutrophil concentration is low, the elimination of the G-CSF is mainly renal and the solution closely tracks the results from the purely renal elimination simulation. But as soon as the circulating neutrophil concentrations get high enough the elimination of G-CSF by binding becomes dominant and quickly drives the G-CSF concentration to very low levels. Similar results are seen if our full neutrophil model (1)–(3) is coupled to (20) with  $\tilde{N}(t) = [N_R(t) + N(t)]$ .

The tendency of the internalisation term to quickly drive the G-CSF concentrations down, along with the propensity for parameter fitting with linear scales resulted in several previous models using versions of (20) to take kinetic parameters for which the elimination of G-CSF is always renal dominated. This is seen both when the G-CSF kinetics is coupled to physiological models as in [5, 11] and when using traditional empirical models as in [69, 30], which consequently all have elimination dynamics which are always renal dominated.

This is true in both the models of Craig [11], which used (20) with  $\tilde{N}(t) = N(t)$ , and Krzyzanski [30] which used an equation similar to (20) but taking account of binding to all available receptors. In both, elimination by internal-

isation is included in the mathematical models but occurs at an insignificant rate compared to the renal elimination, contrary to the clinical understanding that elimination of G-CSF by internalisation is the dominant removal mechanism at homeostasis.

From our numerical experiments it seems impossible to fit the single G-CSF equation (20) to data when  $\tilde{N}(t)$  is taken to be  $N(t)$ . The mature marrow neutrophil reservoir is an order of magnitude larger than the total blood neutrophil pool, and the receptors on the mature neutrophils need to be taken into account in the kinetics as in (4),(5) to obtain a good fit to data. But taking account of all the receptors is not sufficient to obtain a model that fits the physiology closely. This is evidenced by the very poor fit obtained in Figure 2 when coupling our neutrophil model to the reduced G-CSF equation (20) with  $\tilde{N}(t) = [N_R(t) + N(t)]$ , and also from models such as that of Krzyzanski [30] that take account of the G-CSF receptors in marrow, but still obtain renal dominated kinetics.

The study of congenital diseases like cyclical neutropenia (CN)—an inherently oscillatory and dynamic disease— and exogenous dosing regimens (such as during chemotherapy) necessitate that the dynamics of G-CSF be well-characterised. Hence we use the more realistic model (4),(5) for G-CSF pharmacokinetics rather than the single equation reduction (20).

### 3.3 Modelling Granulopoiesis

The first term on the right hand side of (2) gives the rate that mature neutrophils enter the bone marrow reservoir at time  $t$ , and is obtained by modelling the differentiation of stem cells at time  $t - \tau_N(t)$  through mitosis of neutrophil precursors to time  $t - \tau_N(t) + \tau_{N_p} = t - \tau_{N_M}(t)$  followed by maturation of the cells until time  $t$ . The time variation of  $\tau_N(t)$  and  $\tau_{N_M}(t)$  is solution dependent so this term involves state-dependent delays. Granulopoiesis models incorporating state-dependent delay have been employed before in [20, 19, 5], but the derivation of those models was inaccurate and they missed the important  $V_{N_M}(G_1(t))/V_{N_M}(G_1(t - \tau_{N_M}(t)))$  term. Here we will show in detail how the mitotic and maturation stages of the neutrophil precursors can be modelled by age-structured PDE models, whose solution by the method of characteristics leads to the state-dependent delay terms in (2).

We do not model the cell-cycle process during mitosis, nor do we differentiate between the different maturation stages of dividing cells (myeloblasts, promyelocytes, myelocytes). Rather, to simplify the modelling and the resulting differential equations we model mitosis as an exponential process from the moment the HSC commits to differentiate to the end of the mitosis. The proliferation rate  $\eta_{N_p}$  is assumed to be independent of which stage in mitosis the cell has reached. There is evidence that the cytokine G-CSF affects the differentiation of HSCs and the effective proliferation rate during mitosis, as explained in [17], and so we allow both the differentiation rate  $\kappa$  and the prolif-

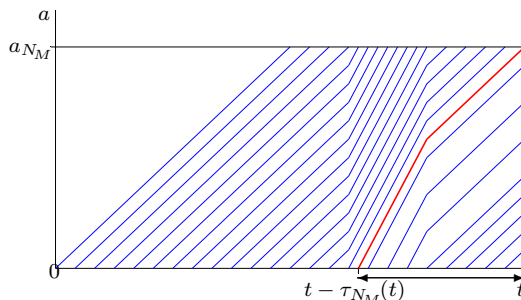


Fig. 3: During maturation the aging rate is variable with  $\dot{a}(t) = V_{N_M}(G_1(t))$ , so age is not trivially related to time, and the maturation time  $\tau_{N_M}(t)$  is variable.

eration rate  $\eta_{N_P}$  to vary with  $G_1$ , the circulating G-CSF, as seen in equations (8),(9), and explained in Section 3.4.

We let  $n_p(t, a)$  be the cell density as a function of time  $t$  and age  $a$  during proliferation. We assume that cells age at a constant rate,  $\dot{a} = 1$ , from age 0 to age  $\tau_{N_P}$ , so  $\tau_{N_P}$  is also the time period that cells spend in proliferation, and the proliferation rate is  $\tau_{N_P}(G_1(t))$ . Then, differentiating,

$$\eta_{N_P}(G_1(t))n_p(t, a) = \frac{dn_p}{dt} = \frac{\partial n_p}{\partial t} + \frac{da}{dt} \frac{\partial n_p}{\partial a} = \frac{\partial n_p}{\partial t} + \frac{\partial n_p}{\partial a}$$

so the age-structured PDE model for proliferation is

$$\frac{\partial n_p}{\partial t} + \frac{\partial n_p}{\partial a} = \eta_{N_P}(G_1(t))n_p(t, a), \quad t \geq 0, \quad a \in [0, \tau_{N_P}], \quad (21)$$

which, by the method of characteristics has solution

$$n_p(t, a) = n_p(t - a, 0) \exp \left[ \int_{t-a}^t \eta_{N_P}(G_1(s)) ds \right], \quad t \geq 0, \quad a \in [0, \min\{t, \tau_{N_P}\}]. \quad (22)$$

If  $\tau_{N_P} \geq a > t > 0$  the solution depends on the initial condition  $n_p(0, a - t)$ , but a similar expression applies. Here we have taken homeostasis as the initial condition throughout and so the solution in (22) is all that is required.

We model the maturing neutrophil precursors (metamyelocytes and bands) as a single homogeneous compartment. There is evidence that G-CSF affects the time that cells spend in maturation [63,3] and the speed up in maturation has been measured experimentally [44]. Since the exact mechanism by which G-CSF affects maturation time is unknown, we will model this process by decoupling time from age and demanding that cells age by an amount  $a_{N_M}$ , but allowing them to mature at a variable aging rate  $\dot{a}(t) = V_{N_M}(G_1(t))$  where  $V_{N_M}(G_1)$  is a monotonically increasing function with  $V_{N_M}(0) > 0$  and  $\lim_{G_1 \rightarrow \infty} V_{N_M}(G_1) = V_{max} < \infty$ .

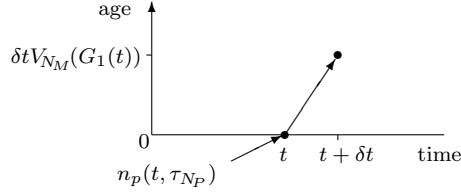


Fig. 4: Transition from proliferation to maturation.

See Section 3.4 for further discussion of the function  $V_{N_M}(G_1)$ . We assume that the rate of cell death,  $\gamma_{N_M}$ , during maturation is constant independent of the concentration of G-CSF.

We let  $n_m(t, a)$  be the cell density as a function of time  $t$  and age  $a$  during maturation for  $t \geq 0$  and  $a \in [0, a_{N_M}]$ . Then the age-structured maturation model is

$$\frac{\partial n_m}{\partial t} + V_{N_M}(G_1(t)) \frac{\partial n_m}{\partial a} = \frac{\partial n_m}{\partial t} + \frac{da}{dt} \frac{\partial n_m}{\partial a} = \frac{dn_m}{dt} = -\gamma_{N_M} n_m(t, a). \quad (23)$$

The characteristics are defined by  $\dot{a} = V_{N_M}(G_1(t))$ , and along characteristics for  $t \geq \tau_{N_M}(t)$  we obtain

$$n_m(t, a_{N_M}) = n_m(t - \tau_{N_M}(t), 0) e^{-\gamma_{N_M} \tau_{N_M}(t)}. \quad (24)$$

Age-structured PDE models have been used in hematopoiesis models many times previously [33, 20, 9, 11], but special care needs to be taken to interpret  $n_m(t, a)$  when the maturation has variable velocity, or an incorrect solution will be obtained.

Cells which mature at time  $t$  enter maturation at time  $t - \tau_{N_M}(t)$  and so differentiated from HSCs at time  $t - \tau_{N_M}(t) - \tau_{N_P} = t - \tau_N(t)$ . The rate at which cells differentiate at time  $t - \tau_N(t)$  is  $\kappa(G_1(t - \tau_N(t)))Q(t - \tau_N(t))$ , and hence

$$n_p(t - \tau_N(t), 0) = \kappa(G_1(t - \tau_N(t)))Q(t - \tau_N(t)).$$

Then by (22)

$$\begin{aligned} n_p(t - \tau_{N_M}(t), a_{N_M}) &= n_p(t - \tau_N(t), 0) \exp \left[ \int_{t - a_{N_M}}^t \eta_{N_P}(G_1(s)) ds \right] \\ &= \kappa(G_1(t - \tau_N(t)))Q(t - \tau_N(t)) \exp \left[ \int_{t - a_{N_M}}^t \eta_{N_P}(G_1(s)) ds \right]. \end{aligned} \quad (25)$$

To obtain the boundary condition for the maturation phase, note that  $n_p(t, \tau_{N_P})$  is the rate at which cells leave proliferation and enter maturation. Hence, to leading order,  $n_p(t, \tau_{N_P})\delta t$  cells enter maturation in the time interval  $[t, t + \delta t]$ . Cells that enter maturation at time  $t$  will already have age  $V_{N_M}(G_1(t))\delta t$  by time  $t + \delta t$ . Since  $n_p(t, a)$  and  $n_m(t, a)$  describe the density of cells in the proliferation and maturation phases, to avoid the spontaneous

creation or destruction of cells at the transition between proliferation and maturation we require

$$\int_0^{V_{N_M}(G_1(t))\delta t} n_m(t + \delta t, a) da - \int_t^{t+\delta t} n_p(t, \tau_{N_P}) dt = \mathcal{O}(\delta t^2).$$

Then

$$\begin{aligned} V_{N_M}(G_1(t))n_m(t, 0) &= \lim_{\delta t \rightarrow 0} \frac{1}{\delta t} \int_0^{V_{N_M}(G_1(t))\delta t} n_m(t + \delta t, a) da \\ &= \lim_{\delta t \rightarrow 0} \frac{1}{\delta t} \int_t^{t+\delta t} n_p(t, \tau_{N_P}) dt = n_p(t, \tau_{N_P}), \end{aligned} \quad (26)$$

and hence the boundary condition for the maturation compartment is

$$n_m(t - \tau_{N_M}(t), 0) = n_p(t - \tau_{N_M}(t), \tau_{N_P})/V_{N_M}(G_1(t - \tau_{N_M}(t))). \quad (27)$$

Combining (24), (25), (27) and (14) we obtain

$$\begin{aligned} n_m(t, a_{N_M}) &= \frac{n_p(t - \tau_{N_M}(t), \tau_{N_P})}{V_{N_M}(G_1(t - \tau_{N_M}(t)))} e^{-\gamma_{N_M}\tau_{N_M}(t)} \\ &= \frac{\kappa(G_1(t - \tau_N(t)))Q(t - \tau_N(t))}{V_{N_M}(G_1(t - \tau_{N_M}(t)))} \exp \left[ \int_{t - \tau_N(t)}^{t - \tau_{N_M}(t)} \eta_{N_P}(G_1(s)) ds - \gamma_{N_M}\tau_{N_M}(t) \right] \\ &= \frac{\kappa(G_1(t - \tau_N(t)))Q(t - \tau_N(t))}{V_{N_M}(G_1(t - \tau_{N_M}(t)))} A_N(t). \end{aligned} \quad (28)$$

Again because of the variable aging-rate there is a correction factor to apply to  $n_m(t, a_{N_M})$  to obtain the rate that cells leave maturation. To calculate this rate notice that cells which reach age  $a_{N_M}$  at time  $t$  have age  $a_{N_M} - V_{N_M}(G_1(t))\delta t + \mathcal{O}(\delta t^2)$  at time  $t - \delta t$ . Thus the number of neutrophils that mature in the time interval  $[t - \delta t, t]$  is

$$\int_{a_{N_M} - V_{N_M}(G_1(t))\delta t}^{a_{N_M}} n_m(t - \delta t, a) da + \mathcal{O}(\delta t^2) = V_{N_M}(G_1(t))n_m(t, a_{N_M})\delta t + \mathcal{O}(\delta t^2).$$

Hence, the rate that cells leave maturation is  $V_{N_M}(G_1(t))n_m(t, a_{N_M})$ , which using (28) can be written as

$$\kappa(G_1(t - \tau_N(t)))Q(t - \tau_N(t))A_N(t) \frac{V_{N_M}(G_1(t))}{V_{N_M}(G_1(t - \tau_{N_M}(t)))}, \quad (29)$$

which is the first term on the right-hand side of (2). The correction factor  $V_{N_M}(G_1(t))/V_{N_M}(G_1(t - \tau_{N_M}(t)))$  was omitted from the state-dependent DDE models in [20, 5].

### 3.4 G-CSF Pharmacodynamics

G-CSF in concert with many other cytokines regulates important parts of granulopoiesis. The precise mechanisms by which it does this are not fully understood (and would probably be beyond the level of detail that we would want to model mathematically even if they were) but it is known that G-CSF acts along several signalling pathways in complex processes which activate and generate secondary signals that regulate neutrophil production [23, 59, 70].

The initiation of signalling pathways and the transfer of the resulting signals responsible for the various effects of a given drug may be driven directly by receptor binding and/or the internalisation of the drug. Assuming the rate at which a drug is internalised is proportional to its bound concentration, we do not need to distinguish between the different possible pathways and will use the concentration of the bound drug to drive the pharmacodynamics and produce the effects in the body.

Many previous models applied the cytokine paradigm mentioned in the introduction to model cytokine effects directly from the circulating neutrophil concentrations. For example in [8, 9, 20, 33, 5, 11], the differentiation function was taken to be a monotonically decreasing function of the circulating neutrophil concentration. Some authors preferred instead to introduce simplified pharmacodynamic models using direct and indirect PD effects related to the concentration of unbound G-CSF [69, 60] while other more detailed approaches have also been studied [58, 66, 65].

The cytokine paradigm breaks down when G-CSF is given exogenously. Immediate responses of the hematopoietic system to G-CSF administration include releasing neutrophils from the marrow reservoir into circulation, and increasing the maturation speed of neutrophils, so the circulating concentration of neutrophils and the total number of neutrophils in the reservoir and circulation both increase, which results in G-CSF and neutrophil concentrations being high concurrently. Consequently we will use G-CSF concentrations from (4),(5) to directly model the pharmacodynamic effects of G-CSF on the differentiation rate of HSCs  $\kappa$ , the effective proliferation rate of neutrophil precursors in mitosis  $\eta_{N_P}$ , the aging rate of maturing neutrophils  $V_{N_M}$ , and the release rate of neutrophils from the bone marrow reservoir  $\varphi_{N_R}$ .

We use Hill and Michaelis-Menten functions to model the G-CSF dependency of these effects. There is some disagreement in the literature over exactly which cytokines are important in different parts of the process, and we may be assigning some effects to G-CSF that are actually due to GM-CSF or one of the other myriad of cytokines that regulate granulopoiesis. If these other cytokines are mostly in quasi-equilibrium with G-CSF, using G-CSF as a cipher for all the cytokines should produce very similar effects without the extraordinary complexity that would be inherent in modelling each one of the cytokines.

Mammalian studies [24, 6, 34] reveal that neutrophils are still produced even in the absence of G-CSF, presumably because other cytokines are acting. Accordingly, we will construct our effects functions to have non-zero activity even in the complete absence of G-CSF. Moreover, in Section 4.3 we will con-



sider the case of G-CSF knockout mathematically with our model to derive a parameter constraint to reduce the number of unknown parameters.

Recall that the concentration of G-CSF bound to mature neutrophils satisfies the inequality  $G_2(t) \leq V[N_R(t) + N(t)]$  with equality only if every G-CSF receptor were bound to two G-CSF molecules. We suppose that the rate that mature neutrophils are released from the marrow reservoir into circulation is dependent on the fraction  $G_{BF}(t) = G_2(t)/(V[N_R(t) + N(t)])$  of their receptors which are bound to G-CSF. The rate is then given by the Michaelis-Menten function  $\varphi_{N_R}(G_1)$  defined by (17). Letting

$$\varphi_{N_R}^{ratio} = \frac{\varphi_{N_R}^{max}}{\varphi_{N_R}^*} > 1, \quad (30)$$

this function is also similar to the one used by Shochat [60] that was adapted in Craig [11] except that we use the fraction of bound receptors to drive the function. At homeostasis (16) and (17) imply that

$$\varphi_{N_R}(G_{BF}^*) = \varphi_{N_R}(G_2^*/[V(N^* + N_R^*)]) = \varphi_{N_R}^*.$$

The parameter  $b_G$  defines the half-effect concentration with

$$\varphi_{N_R}(G_{BF}^* + b_G) = \frac{1}{2}(\varphi_{N_R}^* + \varphi_{N_R}^{max}),$$

while the condition  $\varphi_{N_R}(0) > 0$  implies the constraint

$$b_G > \varphi_{N_R}^{ratio} G_{BF}^* = \frac{G_2^* \varphi_{N_R}^{ratio}}{V(N_R^* + N^*)}. \quad (31)$$

To model the effects of G-CSF on the differentiation, proliferation and maturation some care must be taken. We posit that it is cytokine signalling that drives these processes, and  $G_2(t)$  denotes the concentration of bound G-CSF, which is proportional to the rate that G-CSF is internalised. So it would be tempting to use  $G_2(t)$  to govern these processes, and indeed initially we tried this without success. The problem is that  $G_2(t)$  models the concentration of G-CSF bound to mature neutrophils in the marrow reservoir and circulation. Through (4) and (5) this gives a very good model of the removal of G-CSF from circulation because although the neutrophil progenitor cells also have G-CSF receptors, these cells are relatively few in number and have relatively few receptors, hence they can be ignored when modelling the G-CSF kinetics. However, when modelling the pharmacodynamic effects of G-CSF it appears to be crucial to take account of the binding of G-CSF to the neutrophil precursors, and it is the freely circulating G-CSF which is available to bind to the G-CSF receptors on the immature neutrophils and precursors. Consequently, we should use  $G_1(t)$  to govern the cytokine dependent differentiation, proliferation, and maturation.

Another way to see that it should be the circulating G-CSF  $G_1(t)$ , and not the G-CSF bound to mature neutrophils  $G_2(t)$  that should govern these processes is as follows. If the concentration of mature neutrophils is decreased

then the concentration of bound G-CSF will also decrease because the number of receptors available to bind to will be decreased, but the concentration of unbound G-CSF will increase because the rate the G-CSF is removed by internalisation is reduced. However, with a reduced concentration of neutrophils, an elevated cytokine concentration is needed to increase differentiation, proliferation and maturation speed.

We model the differentiation rate from HSCs to neutrophil precursors using the Hill function (8). Very little is known about how the differentiation rate changes in function of G-CSF, but we suppose that it will not vary by orders of magnitude, since this would lead to instability in the HSC population, while the HSC population is observed to be very stable in healthy subjects [48]. It is then convenient to assume that the homeostatic rate is at the midpoint of the range of possible differentiation rates so

$$\kappa^* = \frac{1}{2}(\kappa^{min} + \kappa^{max}). \quad (32)$$

With this assumption (8) is a standard sigmoidal Hill function with minimum differentiation rate  $\kappa(0) = \kappa^{min}$ , and with  $\kappa(G_1)$  increasing monotonically with  $G_1$  and such that at homeostasis  $\kappa(G_1^*) = \kappa^*$ , while for large concentrations  $\lim_{G_1 \rightarrow \infty} \kappa(G_1) = \kappa^* + (\kappa^* - \kappa^{min}) = \kappa^{max}$ . To ensure that neutrophils are still produced in the complete absence of G-CSF we will require that  $\kappa^{min} > 0$ .

G-CSF is believed to increase the effective rate of mitosis during proliferation by reducing apoptosis. Thus we use a monotonically increasing Michaelis-Menten function  $\eta_{NP}(G_1(t))$  defined by (9) to describe the G-CSF dependent effective proliferation rate (which measures the difference between actual proliferation and apoptosis). This function looks a little different than the other Michaelis-Menten functions we will use, but this is simply because it has been scaled to give the correct minimal and homeostasis effects with  $\eta_{NP}(0) = \eta_{NP}^{min} > 0$  and  $\eta_{NP}(G_1^*) = \eta_{NP}^*$ , with  $\eta_{NP}(G_1)$  a monotonically increasing function of  $G_1$ .

Letting

$$\eta_{NP}^{max} = \lim_{G_1 \rightarrow \infty} \eta_{NP}(G_1) = \eta_{NP}^* + \frac{b_{NP}}{G_1^*}(\eta_{NP}^* - \eta_{NP}^{min}),$$

we see that

$$\frac{b_{NP}}{G_1^*} = \frac{\eta_{NP}^{max} - \eta_{NP}^*}{\eta_{NP}^* - \eta_{NP}^{min}},$$

so the parameter  $b_{NP} > 0$  determines the relative position of  $\eta_{NP}^* \in [\eta_{NP}^{min}, \eta_{NP}^{max}]$  with  $\eta_{NP}^* > (\eta_{NP}^{min} + \eta_{NP}^{max})/2$  when  $b_{NP} \in (0, G_1^*)$  and  $\eta_{NP}^* < (\eta_{NP}^{min} + \eta_{NP}^{max})/2$  when  $b_{NP} > G_1^*$ .

G-CSF is known to affect the time that neutrophils spend in maturation [63, 3], an acceleration in maturation that Price [44] measured experimentally, but the mechanism by which G-CSF speeds up maturation is not well understood. We choose to model this process by decoupling time from age and demanding that cells age by an amount  $a_{NM}$ , but allowing them to mature

at a variable aging rate  $\dot{a}(t) = V_{N_M}(G_1(t))$  where  $V_{N_M}(G_1)$  is a monotonically increasing Michaelis-Menten function given in (10). This is similar to the form used in Craig [11] which was adopted from Foley [20], and is also functionally equivalent to (17).

$b_V$  is the half effect parameter for the aging velocity with  $V_{N_M}(G_1^* + b_V) = (1 + V_{max})/2$ . We require that  $V_{N_M}(0) > 0$ , which from (10) is equivalent to

$$b_V > G_1^* V_{max}. \quad (33)$$

This constraint ensures that the aging velocity  $V_{N_M}(G_1)$  is strictly positive for all  $G_1 \geq 0$ . The function  $V_{N_M}(G_1)$  also satisfies the homeostasis condition  $V_{N_M}(G_1^*) = 1$ , so that at homeostasis the aging rate is 1. The aging rate saturates with  $\lim_{G_1 \rightarrow \infty} V_{N_M}(G_1) = V_{max} < \infty$ .

Notice that, using (13)

$$\frac{d}{dt}(t - \tau_{N_M}(t)) = 1 - \frac{d}{dt}\tau_{N_M}(t) = \frac{V_{N_M}(G_1(t))}{V_{N_M}(G_1(t - \tau_{N_M}(t)))}, \quad (34)$$

and positivity of  $V_{N_M}(G_1)$  assures that  $t - \tau_{N_M}(t)$ , and similarly  $t - \tau_N(t)$ , are monotonically increasing functions of  $t$ . This is important in state-dependent DDE theory for existence and uniqueness of solutions. Physiologically, it assures that cells which have exited proliferation or maturation never re-enter those phases.

The responses of our new model and the model of Craig [11] to exogenous administration of G-CSF are very different. With our new model both differentiation and proliferation are increased with increased G-CSF so that after some time delay the marrow reservoir gets replenished. In the previous model, the G-CSF triggered an immediate release of neutrophils from the marrow reservoir into circulation and the resulting high circulating neutrophil count would cause differentiation and proliferation to be decreased. This meant the the marrow reservoir would suffer a double depletion with increased release into circulation combined with reduced production of new mature neutrophils, which could lead to instabilities in the model that ought not to be occurring in the granulopoiesis of healthy subjects.

Since the four functions (8),(9),(10) and (17) describe the effects of G-CSF on granulopoiesis, rather than modelling the processes that lead to the effects, the parameters in these functions do not correspond to physiological quantities that can be measured directly. Nevertheless these parameters can be determined by fitting the response of the system to experimental data as described in Section 4.4.

### 3.5 Modelling exogenous drug administration

As noted following (4),  $I_G(t)$  denotes the input of exogenous G-CSF. The administration of rhG-CSF (in our case filgrastim) typically takes two forms: IV infusion (where the drug is given intravenously over a period of time)

or subcutaneously (injection under the skin). In the former case, the drug passes directly into the bloodstream meaning the bioavailable fraction (the percentage of the administered dose that enters the blood) is 100%. In this case, we express the single exogenous administration as

$$I_G(t) = \begin{cases} \frac{Do}{t_{inf}V_d}, & t_0 \leq t \leq t_{inf} \\ 0 & \text{otherwise,} \end{cases} \quad (35)$$

where  $Do$  is the administered dose,  $t_0$  is the start of the infusion,  $t_{inf}$  is the time of infusion and  $V_d$  is the volume of distribution. The volume of distribution is a pharmacokinetic parameter which relates the hypothetical volume a drug would occupy to the concentration it is observed in the plasma. It is typically calculated for a drug by dividing the administered dose by the concentration in the blood immediately following an administration for the simplest case of IV bolus administration (instantaneous administration into the blood). Drugs given subcutaneously do not immediately reach the bloodstream. Instead, a certain proportion of the medication remains in the subcutaneous tissue pool before diffusing into the plasma. Some previous studies, notably [20, 5] used an extra transition compartment to model the administered G-CSF concentration in the tissues before reaching the blood and allowed for the free exchange between this central (blood) compartment and the tissue compartment. Owing to the specifics of the pharmacokinetics of filgrastim, we will instead use the following direct input functions from [30] and [11] to model subcutaneous administration as

$$I_G(t) = \begin{cases} \frac{k_a Do F}{V_d} e^{k_a t}, & t \geq t_0 \\ 0 & t < t_0, \end{cases} \quad (36)$$

where  $k_a$  is the constant of absorption, and  $F$  is the bioavailable fraction (the fraction of non-metabolised dose which enters the system). This direct form is preferred over the two compartment method previously employed in [20, 5] because of the relatively small volume of distribution exhibited by filgrastim (the bio-similar exogenous form of G-CSF), which is to say that  $V_d$  is less than the standard 70L measure of highly distributed drugs [11] and that the drug does not have a strong tendency to redistribute into the tissues.

The pharmacokinetic model of the chemotherapeutic drug (Zalypsis<sup>®</sup>) used in this paper is the same as in [11]. Briefly, the concentration of chemotherapeutic drug in the system is modelled using a set of four ordinary differential equations which was determined to be suitable through population pharmacokinetic analysis [41]. The PK model of Zalypsis<sup>®</sup> is given by

$$\begin{aligned} \frac{d}{dt} C_p(t) &= I_C(t) + k_{fp} C_f(t) + k_{sl_1 p} C_{sl_1}(t) - (k_{pf} + k_{psl_1} + k_{el_C}) C_p(t) \\ \frac{d}{dt} C_f(t) &= k_{pf} C_p(t) + k_{sl_2 f} C_{sl_2}(t) - (k_{fp} + k_{fsl_2}) C_f(t) \\ \frac{d}{dt} C_{sl_1}(t) &= k_{psl_1} C_p(t) - k_{sl_1 p} C_{sl_1}(t), \quad \frac{d}{dt} C_{sl_2}(t) = k_{fsl_2} C_f(t) - k_{sl_2 f} C_{sl_2}(t), \end{aligned} \quad (37)$$

where  $C_p$  is the concentration in the central (blood) compartment,  $C_f$  is the concentration in the fast-exchange tissues, and  $C_{sl_1}$  and  $C_{sl_2}$  are the concentrations in the slow-exchange tissues,  $k_{ij}$  are traditional rate constants between

the  $i^{th}$  and  $j^{th}$  compartments ( $i, j = p, f, sl_1, sl_2$ ), and  $k_{elC}$  is the rate of elimination from the central compartment. We consider the chemotherapeutic drug to be administered by IV infusion, so  $I_C(t) = Dose_{Zal}/\Delta_t$ , where  $Dose_{Zal}$  is the administered dose and  $\Delta_t$  is the time of infusion.

In contrast to the pharmacodynamic effects of G-CSF, chemotherapy has negative effects on the neutrophil (and other blood) lineages. Chemotherapy (and radiotherapy) works by disrupting the cell-cycle of tumours [37] but this interference also affects all cells which are dividing, including the neutrophil progenitors. The cytotoxic side effects chemotherapeutic treatment has on the neutrophils is called myelosuppression and it is a leading cause of treatment adaptation and/or cessation for patients undergoing chemotherapy [11]. Since chemotherapy's myelosuppressive action only affects cells capable of division, we model the pharmacodynamic effects of chemotherapy on the HSCs, which rarely divide, and the neutrophil progenitors in the proliferative phase, which divide regularly until they exit the mitotic phase.

Since the effects of chemotherapy on the HSCs are not clear, we model the antiproliferative effect as a simple linear decrease of the rate of apoptosis experienced by these cells by replacing  $\gamma_Q$  in equation (18) by  $\gamma_Q + h_Q C_p(t)$  where  $C_p(t)$  is the concentration of the chemotherapeutic drug in the central blood compartment given by (37), and  $h_Q$  is a factor to be determined (as outlined in Section 4.5). Then (18) gives

$$A_Q(t) = 2e^{-\gamma_Q \tau_Q - h_Q \int_{t-\tau_Q}^t C_p(s) ds}. \quad (38)$$

It is convenient to numerically implement (38) as a differential equation, and applying Leibniz's Rule to (38), similar to the derivation of (15), we obtain

$$\frac{d}{dt} A_Q(t) = (h_Q (C_p(t - \tau_Q) - C_p(t))) A_Q(t), \quad (39)$$

and we replace (7) by (39) when chemotherapy is administered.

The second effect of chemotherapeutic drugs is to reduce the effective proliferation rate of the mitotic neutrophil progenitors. We model this by replacing  $\eta_{Np}$  of (9) by

$$\eta_{Np}^{chemo}(G_1(t), C_p(t)) = \eta_{Np}^{inf} + \frac{\eta_{Np}(G_1(t)) - \eta_{Np}^{inf}}{1 + (C_p(t)/EC_{50})^{s_c}}, \quad (40)$$

which is a modification of the model used in [11]. Here  $\eta_{Np}^{inf}$  corresponds to the effective proliferation rate in the presence of an infinite dose of the drug. We require  $\eta_{Np}^{inf} < \eta_{Np}^{min}$  to ensure that effective proliferation is reduced, so  $\eta_{Np}^{chemo}(G_1(t), C_p(t)) < \eta_{Np}^{chemo}(G_1(t))$  whenever  $C_p(t) > 0$ . We will allow the possibility of  $\eta_{Np}^{inf} < 0$ , which would correspond to negative effective proliferation (more death than division in the mitotic phase) in the presence of very large concentrations of the chemotherapeutic drug, though we note that because the drug is cleared from circulation relatively quickly we will have  $\eta_{Np}^{chemo}(G_1(t), C_p(t)) > 0$  most of the time even if  $\eta_{Np}^{inf} < 0$ . If  $\eta_{Np}^{inf} \in (0, \eta_{Np}^{min})$  then effective cell division is reduced but never completely halted however large

the concentration of the chemotherapeutic drug.  $EC_{50}$  is the concentration of chemotherapeutic drug which gives the half-maximal effect, and  $s_c$  is a Hill coefficient. The parameters  $h_Q$ ,  $\eta_{N_P}^{inf}$ ,  $EC_{50}$ , and  $s_c$  will all be estimated using fitting techniques described in Section 4.5.

## 4 Parameter Estimation and Equation Constraints

In this section we show how our mathematical model imposes constraints on its own parameters to be self-consistent, and how experimental data can be used to determine model parameters. We begin in Section 4.1 by studying the model at homeostasis and deriving inequalities that the parameters must satisfy, as well as showing how experimentally measured quantities can be used to directly determine some parameters in the model. In Section 4.2 we show how the G-CSF pharmacokinetic parameters can be determined using a combination of model equation constraints and parameter fitting to experimental data from single administrations of G-CSF. In Section 4.3, G-CSF knockout is used to derive further parameter constraints and relationships. Finally in Section 4.4 we show how the pharmacodynamic parameters in the neutrophil equations can be determined by fitting the model to experimental data for the circulating neutrophil concentrations after a single IV or subcutaneous administration of G-CSF.

### 4.1 Neutrophil Steady-State Parameter Determination and Constraints

At homeostasis let  $Q^*$  be the stem cell concentration and denote the sizes of the four neutrophil compartments at homeostasis by  $N_P^*$  (proliferation),  $N_M^*$  (maturation),  $N_R^*$  (marrow reservoir),  $N^*$  (total blood neutrophil pool), and the average time that a cell spends in one of these stages at homeostasis by  $\tau_{N_P}$ ,  $a_{N_M}$ ,  $\tau_{N_R}^*$  and  $\tau_{N_C}^*$ , respectively. With the exception of  $\tau_{N_P}$ , all of these quantities have been determined experimentally, but unfortunately only  $\tau_{N_P}$  and  $a_{N_M}$  actually appear in our model. In this section we show that our model imposes some constraints on the values of these parameters, and also how the values of  $\kappa^*$ ,  $N_P^*$ ,  $N_M^*$ ,  $N_R^*$ ,  $N^*$ ,  $a_{N_M}$ ,  $\tau_{N_R}^*$  and  $\tau_{N_C}^*$  can be used through the model to determine values for the parameters  $\tau_{N_P}$ ,  $\eta_{N_P}^*$ ,  $\gamma_{N_M}$ ,  $\gamma_{N_R}$ ,  $\gamma_N$  and  $\varphi_{N_R}^*$  which do appear in the model in Section 2.

At homeostasis equations (1)–(3) become

$$0 = -(\kappa^* + \kappa_\delta + \beta(Q^*))Q^* + A_Q^*\beta(Q^*)Q^*, \quad (41)$$

$$\kappa^*Q^*A_N^* = (\varphi_{N_R}^* + \gamma_{N_R})N_R^*, \quad (42)$$

$$\varphi_{N_R}^*N_R^* = \gamma_N N^*. \quad (43)$$

Equation (41) has the trivial solution  $Q^* = 0$  with other solutions given by

$$\kappa^* + \kappa_\delta = (A_Q^* - 1)\beta(Q^*) \quad (44)$$

To the best of our knowledge, there is no experimental data to determine the relative rates of differentiation to the three cell lines (erythrocytes, neutrophils, thrombocytes) at homeostasis. In the absence of any evidence to the contrary, we will assume that these are all equal. Since  $\kappa^*$  denotes the differentiation rate to the neutrophil line and  $\kappa_\delta$  differentiation to erythrocyte and thrombocyte precursors we obtain

$$\kappa^* = \frac{1}{2}\kappa_\delta = \frac{1}{3}(A_Q^* - 1)\beta(Q^*). \quad (45)$$

At homeostasis neutrophil precursors are assumed to enter the mitotic phase at rate  $\kappa^*Q^*$ . They then proliferate at a rate  $\eta_{NP}^*$  for a time  $\tau_{NP}$ . The total number of cells in the proliferative phase at homeostasis is thus

$$N_P^* = \int_0^{\tau_{NP}} \kappa^*Q^* e^{\eta_{NP}^* s} ds = \kappa^*Q^* \frac{e^{\eta_{NP}^* \tau_{NP}} - 1}{\eta_{NP}^*}, \quad (46)$$

and cells leave proliferation and enter maturation at a rate  $R_P^*$  given by

$$R_P^* = \kappa^*Q^* e^{\eta_{NP}^* \tau_{NP}}. \quad (47)$$

At homeostasis from (10) we have  $V_{N_M}(G_2^*) = 1$ , and thus from (11), the time spent in maturation at homeostasis is  $a_{N_M}$ . The number of cells of age  $s$  for  $s \in [0, a_{N_M}]$  in the maturation phase is then  $\kappa^*Q^* \exp(\eta_{NP}^* \tau_{NP} - \gamma_{N_M} s)$ , and the total number of cells in the maturation phase is

$$N_M^* = \int_0^{a_{N_M}} \kappa^*Q^* e^{\eta_{NP}^* \tau_{NP} - \gamma_{N_M} s} ds = \kappa^*Q^* e^{\eta_{NP}^* \tau_{NP}} \frac{1 - e^{-\gamma_{N_M} a_{N_M}}}{\gamma_{N_M}}. \quad (48)$$

Writing

$$A_N^* = \exp(\eta_{NP}^* \tau_{NP} - \gamma_{N_M} a_{N_M}), \quad (49)$$

which corresponds to (14) at homeostasis, we can rewrite (48) as

$$N_M^* = \kappa^*Q^* A_N^* \frac{e^{\gamma_{N_M} a_{N_M}} - 1}{\gamma_{N_M}}. \quad (50)$$

Now the rate at which cells leave the maturation phase is

$$\kappa^*Q^* e^{\eta_{NP}^* \tau_{NP} - \gamma_{N_M} a_{N_M}} = \kappa^*Q^* A_N^*.$$

The average time,  $\tau_{N_C}^*$ , that neutrophils spend in circulation in the blood (in the total blood neutrophil pool) has been measured a number of times. However, what is actually measured is the half removal time,  $\tau_{1/2}$ , which gives  $\gamma_N$ , the removal rate from circulation by

$$\gamma_N = \frac{1}{\tau_{N_C}^*} = \frac{\ln 2}{\tau_{1/2}}. \quad (51)$$

Equation (43) ensures that at homeostasis the rate neutrophils leave the reservoir and enter circulation equals the rate at which they are removed from circulation. From this we obtain

$$\varphi_{N_R}^* = \frac{\gamma_N N^*}{N_R^*}. \quad (52)$$

The rate at which neutrophils exit the mature marrow reservoir is given by  $(\varphi_{N_R}^* + \gamma_{N_R})N_R^*$  where  $\varphi_{N_R}^*$  is the transition rate constant for cells entering circulation and  $\gamma_{N_R}$  is the random death rate. Thus the average time that cells spend in the reservoir at homeostasis is

$$\tau_{N_R}^* = \frac{1}{\varphi_{N_R}^* + \gamma_{N_R}}. \quad (53)$$

Hence the random death rate in the reservoir,  $\gamma_{N_R} \geq 0$ , is given by

$$\gamma_{N_R} = \frac{1}{\tau_{N_R}^*} - \varphi_{N_R}^*, \quad (54)$$

and we require that

$$\tau_{N_R}^* \varphi_{N_R}^* \leq 1 \quad (55)$$

to ensure that  $\gamma_{N_R} \geq 0$ . That said, using (51) and (52), we can rewrite (55) as

$$\frac{\tau_{N_R}^*}{\tau_{N_C}^*} \leq \frac{N_R^*}{N^*}. \quad (56)$$

The apoptosis rate during the maturation phase,  $\gamma_{N_M} \geq 0$ , is calculated by eliminating  $\kappa^* Q^* A_N^*$  from (42) and (50). Also making use of (54), we obtain

$$F_M(\gamma_{N_M}) := N_R^* (e^{\gamma_{N_M} a_{N_M}} - 1) - \gamma_{N_M} \tau_{N_R}^* N_M^* = 0. \quad (57)$$

It is easy to see that  $F_M(0) = 0$  and hence  $\gamma_{N_M} = 0$  is one solution of (57). Since  $F_M''(\gamma) > 0$  for all  $\gamma \geq 0$ , if  $F_M'(0) < 0$  there is a unique  $\gamma_{N_M} > 0$  such that  $F_M(\gamma_{N_M}) = 0$ , and no positive value of  $\gamma$  such that  $F_M(\gamma) = 0$  if  $F_M'(0) \geq 0$ . Since cell death is known to occur in the maturation compartment (see [36]), we should choose our parameters so that (57) admits a solution  $\gamma_{N_M} > 0$ . The condition  $F_M'(0) > 0$  is equivalent to

$$\frac{N_R^*}{N_M^*} < \frac{\tau_{N_R}^*}{a_{N_M}}, \quad (58)$$

and to include apoptosis in the maturation compartment our parameters must be chosen to satisfy (58).

Equation (56) can be interpreted as a lower bound on  $\tau_{N_R}^*$ , and (58) as an upper bound. Eliminating  $\tau_{N_R}^*$  from these two bounds we find that the parameters must satisfy

$$\frac{a_{N_M}}{\tau_{N_C}^*} < \frac{N_M^*}{N^*} \quad (59)$$



for the constraints (56) and (58) to be consistent. Then  $\tau_{NR}^*$  must satisfy

$$\tau_{NR}^* \in \left( a_{NM} \frac{N_R^*}{N_M^*}, \tau_{NC}^* \frac{N_R^*}{N^*} \right) \quad (60)$$

for both (56) and (58) to be satisfied as strict inequalities. All the quantities in (60) have been estimated experimentally. To be consistent with our model the values must satisfy both (59) and (60). In Section 5 we state parameters that satisfy these constraints. With those parameters we take  $\gamma_{NM} > 0$  to be the unique strictly positive solution to (57).

Equation (42) ensures that the rate cells enter and leave the reservoir are equal at homeostasis. Rearranging and using (52) we obtain

$$A_N^* = \frac{N_R^*}{\kappa^* Q^* \tau_{NR}^*}, \quad (61)$$

which determines  $A_N^*$ . Now from (49) we have

$$e^{\eta_{NP}^* \tau_{NP}} = A_N^* e^{\gamma_{NM} a_{NM}}, \quad (62)$$

which determines  $e^{\eta_{NP}^* \tau_{NP}}$ , and it remains to determine one of  $\eta_{NP}^*$  or  $\tau_{NP}$  in order to be able to find the other. However (46) implies that

$$\eta_{NP}^* = \kappa^* Q^* \frac{e^{\eta_{NP}^* \tau_{NP}} - 1}{N_P^*} = \kappa^* Q^* \frac{A_N^* e^{\gamma_{NM} a_{NM}} - 1}{N_P^*} \quad (63)$$

and now from (62) we have

$$\tau_{NP} = \frac{1}{\eta_{NP}^*} \ln(A_N^* e^{\gamma_{NM} a_{NM}}). \quad (64)$$

In Section 5 we use the equations of this section to determine parameter values for our model.

## 4.2 Estimation of G-CSF Pharmacokinetic Parameters

Following [71, 26, 2, 30] we take the homeostasis concentration of the free circulating G-CSF to be  $G_1^* = 0.025$  ng/mL. The parameter  $V$  in (5) is the same parameter  $V$  as appears in (20). But  $V$  is difficult to interpret directly from (20), and although published values are available, they vary widely between sources. For the pharmacokinetic G-CSF model (4),(5) the meaning of  $V$  is clear; its simply the conversion factor that converts a neutrophil concentration  $N$  in units of  $10^9$  cells per kilogram of body mass, into the corresponding G-CSF concentration  $VN$  in units of nanograms per millilitre when every receptor on the neutrophils is bound.

To compute  $V$ , we first note that the molecular mass of G-CSF is  $18.8$  kDa =  $18800$  g/mol [30] or dividing by Avogadro's constant, the equivalent weight of G-CSF is  $G_{mw} = 3.12 \times 10^{-11}$  ng/molecule. We take the number of receptors

per neutrophil to be  $R = 600$ , which is in the middle of the range that Barreda [2] cites, though we note that both smaller and larger numbers can be found in the literature. Then given  $N$ , the number of receptors per millilitre is

$$R \times \frac{70}{5000} \times 10^9 \times N,$$

where we assume body mass of 70 kg and 5000 mL of blood. Since two molecules bind to each receptor the maximum concentration of bound G-CSF is

$$VN = 2 \times G_{mw} \times R \times \frac{70}{5000} \times 10^9 \times N = 0.525N \text{ ng/mL}$$

and hence

$$V = 0.525 (\text{ng/mL}) / (10^9 \text{ cells/kg}). \quad (65)$$

Values have been published for several of the other parameters in the G-CSF equations (4),(5), but these have been largely based on *in vitro* experiments and/or simpler G-CSF models using mixed-effects estimation techniques, and so are not directly applicable to our model [30,69,58,52].

At homeostasis, equations (4),(5) give

$$G_2^* = \frac{(G_1^*)^{Pow}}{(G_1^*)^{Pow} + (k_{int} + k_{21})/k_{12}} V [N_R^* + N^*], \quad (66)$$

and

$$\begin{aligned} G_{prod} &= k_{ren} G_1^* + k_{int} G_2^* \\ &= k_{ren} G_1^* + k_{int} V [N_R^* + N^*] \frac{(G_1^*)^{Pow}}{(G_1^*)^{Pow} + (k_{int} + k_{21})/k_{12}}. \end{aligned} \quad (67)$$

Once values of  $k_{int}$ ,  $k_{12}$ ,  $k_{21}$ ,  $k_{ren}$  and  $Pow$  are determined as we describe below, (66) and (67) determine values for  $G_2^*$  and  $G_{prod}$ .

The remaining parameters might be determined by simulating the full model with exogenous G-CSF administration and fitting the response of the model to published data for such experiments. However, that would involve also fitting the as yet undetermined pharmacodynamic parameters in equations (1)–(17) which would create a very large optimisation problem, with the potential for interactions between the pharmacokinetic and pharmacodynamic parameters to create a complicated functional with many local minima. To avoid this, we prefer to determine the pharmacokinetic and pharmacodynamic parameters separately. Here we determine the PK parameters by decoupling the G-CSF equations (4)–(5) from the neutrophil dynamics.

There have been a number of studies tracking the response of the hematopoietic system to a single administration of exogenous G-CSF including Wang [69] and Krzyzanski [30]. If data were available for circulating neutrophil and marrow reservoir neutrophil concentrations as functions of time it would be possible to treat equations (4)–(5) separately from the rest of the model as a system of two ordinary differential equations with  $[N_R(t) + N(t)]$  treated as a known

non-autonomous forcing term determined by the data. But unfortunately it is not known how to directly measure either marrow neutrophil reservoir or bound G-CSF concentrations, and such values are not reported in the literature.

In the absence of marrow neutrophil data we will decouple the G-CSF kinetic equations (4)-(5) from the rest of the model by replacing the time dependent term  $[N_R(t) + N(t)]$  by the constant  $N_{tot}$  to obtain

$$\begin{aligned} \frac{d}{dt}G_1(t) &= I_G(t) + G_{prod} - k_{ren}G_1(t) \\ &\quad - k_{12}(N_{tot}V - G_2(t))G_1(t)^{Pow} + k_{21}G_2(t) \end{aligned} \quad (68)$$

$$\frac{d}{dt}G_2(t) = -k_{int}G_2(t) + k_{12}(N_{tot}V - G_2(t))G_1(t)^{Pow} - k_{21}G_2(t). \quad (69)$$

In (68) and (69) the constant  $N_{tot}$  represents the constant total number of neutrophils available for G-CSF binding, and will be treated as an extra parameter to be determined during the fitting. It should correspond approximately to an average value of  $[N_R(t) + N(t)]$  across the time course of the data.

With data for bound G-CSF unavailable we are constrained to fit (68), (69) to data for the unbound G-CSF. To do this we use digitisations of two sets of data from Wang [69] from a 750  $\mu\text{g}$  intravenous (IV) administration of G-CSF and from a subcutaneous (SC) administration of the same dose. SC administrations necessarily include the absorption kinetics of a drug, as outlined in equation (36), whereas IV administrations reach the blood directly and can be modelled more simply as in (35). For these reasons, both IV and SC data were used simultaneously during the fitting procedure to best characterise the parameters. Rather than fitting directly to the data from Wang [69], to obtain robust parameter fits we took the G-CSF data from the SC and IV administrations and fit a spline through each to define functions  $G_{dat}^{SC}(t)$  and  $G_{dat}^{IV}(t)$  over the time intervals  $0 \leq t \leq 2$  days for which the data were taken. With postulated parameter values we then use the Matlab [38] ordinary differential equation solver *ode45* to simulate (68), (69) over the same time interval to define functions  $G_1^{SC}(t)$  and  $G_1^{IV}(t)$ . We measure the error between the simulated solutions and the data using the  $L^2$  function norm defined by

$$\|G\|_2^2 = \int_0^T G(t)^2 dt. \quad (70)$$

For the IV data which varies over orders of magnitude, as seen in Figure 2, we use a log scale, while for the SC data a linear scale is appropriate. We define a combined error function for both simulations by

$$Err = \|\log(G_1^{IV}) - \log(G_{dat}^{IV})\|_2^2 + \chi^{0.95} \|G_1^{SC} - G_{dat}^{SC}\|_2^2, \quad (71)$$

where the scale factor  $\chi$  defined by

$$\chi = \frac{\max_{t \in [0, T]} \log(G_{dat}^{IV}(t)) - \min_{t \in [0, T]} \log(G_{dat}^{IV}(t))}{\max_{t \in [0, T]} G_{dat}^{SC}(t) - \min_{t \in [0, T]} G_{dat}^{SC}(t)}, \quad (72)$$

effectively rescales the data so that both data sets have equal weight. (Since  $\chi < 1$  the power 0.95 in (71) works to give slightly more weight to the SC data).

Fitting was performed using the Matlab [38] *lsqcurvefit* least squares solver, with the error function  $Err$  evaluated numerically by sampling the functions at a thousand equally spaced points. It is convenient to define the constant

$$N_{elim} = 1 - \frac{k_{ren}G_1^*}{G_{prod}} \quad (73)$$

where  $N_{elim}$  is the fraction of G-CSF clearance performed through internalisation at homeostasis (obtained in (73) as one minus the fraction of renal clearance at homeostasis). The estimation was performed for the G-CSF parameters:  $k_{12}$ ,  $k_{21}$ ,  $Pow$ ,  $k_{int}$ , the neutrophil constant  $N_{elim}$ , and the pharmacokinetic drug parameters  $k_a$ , and  $F$ . The elimination fraction  $N_{elim}$  was either fixed ( $N_{elim} = 0.6$  and  $0.8$  in Table 1) or fitted (the other entries in Table 1). At each step of the optimisation the candidate  $k_{12}$ ,  $k_{21}$ ,  $Pow$ ,  $k_{int}$  and  $N_{elim}$  are used to determine the dependent parameters  $G_2^*$ ,  $k_{ren}$ , and  $G_{prod}$ , which from (68), (69) and (73) are given by

$$G_2^* = VN_{tot} \frac{(G_1^*)^{Pow}}{(G_1^*)^{Pow} + (k_{21} + k_{int})/k_{12}} \quad (74)$$

$$k_{ren} = \left( -1 + \frac{1}{N_{elim}} \right) V k_{int} (G_1^*)^{(Pow-1)} \frac{N_{tot}}{(G_1^*)^{Pow} + (k_{21} + k_{int})/k_{12}} \quad (75)$$

$$G_{prod} = k_{int}G_2^* + k_{ren}G_1^*. \quad (76)$$

The following fitting procedure was employed. First parameters were fit from IV data for a  $750 \mu\text{g}$  administration [69] on the log scale to ensure that behaviour at both high and low concentrations were properly characterised. Next initial SC parameters were fit from  $750 \mu\text{g}$  SC data in linear scale. Using the parameters from these two fits as seed values, we next obtain final parameter values by fitting both log-concentration IV and linear SC data simultaneously using the norm defined in (71). Finally, as the pharmacokinetic parameters related to the SC administration have been shown to be dose-dependent [58], we re-estimate  $F$  and  $k_a$  for lower doses of  $300 \mu\text{g}$  and  $375 \mu\text{g}$  [30, 69]. Since  $V_d$  is typically calculated by the ratio of the dose to the initial concentration in the blood for IV administrations [15], we have applied the same calculation here to scale the G-CSF prediction to the first measured data point. Accordingly, the volume of distribution was recalculated to fit the administered dose. The resulting parameters are reported in Table 1.

Figure 5 compares the solutions from the fitting procedure of the simplified model (68) (69) for the parameter set with  $N_{elim} = 0.80$  from Table 1 to the Wang [69] data for  $750 \mu\text{g}$  IV and SC doses in log and linear scales, respectively.

Figure 6(a-b) gives linear and log scale plots of the simulations of (68), (69) with the  $N_{elim} = 0.80$  parameter set from Table 1 for an IV administration from Krzyzanski [30]. In this case no fitting was performed; the Krzyzanski [30] protocol is simulated using parameters obtained from fitting to the Wang

Name	Value 1	Value 2	Value 3	Value 4	Value 5	Units
$N_{elim}$	0.097478	0.6	0.71678	0.8	0.87358	–
$k_{ren}$	1.3142	0.45064	0.2456	0.16139	0.094597	days <sup>-1</sup>
$k_{12}$	2.3004	2.2519	2.1342	2.2423	2.878	days <sup>-1</sup>
$k_{21}$	407.1641	198.2403	168.2588	184.8658	259.8087	days <sup>-1</sup>
$k_{int}$	394.5111	459.2721	275.2744	462.4209	632.0636	days <sup>-1</sup>
$Pow$	1.7355	1.4418	1.4631	1.4608	1.4815	–
$N_{tot}$	3.9496	4.1767	4.1457	4.2009	3.606	10 <sup>9</sup> cells/kg
$Do = 750 \mu\text{g}, V_d = 2178.0 \text{ mL}$						
$F$	0.99752	0.75	0.75	0.75	0.98271	–
$k_a$	3.8154	5.2142	5.0574	5.143	4.1931	days <sup>-1</sup>
$Err$	0.16352	0.15716	0.17901	0.18543	0.21130	–
$Do = 300 \mu\text{g}, V_d = 4754.7 \text{ mL}$						
$F$	1	0.63361	0.62299	0.64466	0.71424	–
$k_a$	6.3783	8.0804	8.0628	8.0236	7.4367	days <sup>-1</sup>
$Do = 375 \mu\text{g}, V_d = 2322.9 \text{ mL}$						
$F$	0.89831	0.4801	0.48549	0.49964	0.57618	–
$k_a$	4.18161	6.7326	6.6324	6.6133	6.1259	days <sup>-1</sup>

Table 1: Pharmacokinetic parameter estimates from the simplified G-CSF model (68),(69) for different homeostasis elimination fractions of  $N_{elim}$ .  $Err$  is defined by (71) for the 750  $\mu\text{g}$  dose. As described in the text, dose-dependent drug parameters were only recalculated for the lower doses.

data, and a good fit to the data is still obtained. Figure 6(c) shows another simulation for a slightly larger SC dose, with the same G-CSF parameters (only the the dose-dependent drug parameters  $k_a$  and  $F$  were fit, as already noted), and we again obtain good agreement with the data.

Figure 6(d) validates the use of the  $N_{tot}$  simplification used for (68),(69) by comparing  $N_{tot}$  to  $N_R(t) + N(t)$  from the solution of the full model (1)-(17) and to  $N_R^* + N^*$ . This demonstrates how  $N_{tot}$  effectively averages  $N_R(t) + N(t)$  over most of the simulation.

We characterize the parameter sets found for the simplified G-CSF model (68),(69) by the fraction  $N_{elim}$  of the G-CSF that is cleared by binding and internalisation at homeostasis. For  $0 \leq N_{elim} < 1/2$  the elimination is renal dominated at homeostasis, while for  $1/2 < N_{elim} \leq 1$  the pharmacokinetics is internalisation dominant. As already mentioned in Section 3.2, from a clinical standpoint, it is believed that  $N_{elim} > 1/2$ , while a number of previously published models including [11, 30, 69] have  $N_{elim}$  close to zero.

When we included  $N_{elim}$  as a parameter to be fit the results were very sensitive to the seed values used to start the optimisation and had a tendency to produce parameter sets with very low or very high  $N_{elim}$  (see the  $N_{elim} = 0.097$  and  $N_{elim} = 0.87358$  parameter sets in Table 1), but we also found a good fit with  $N_{elim} = 0.71678$  and were able to find good fits for any fixed value of  $N_{elim}$ , as seen in Figure 5 (see Table 1 for parameter sets with  $N_{elim} = 0.6$  and 0.8). Our results seem to indicate that there is at least a one parameter family of plausible parameter sets with each set characterised by the value of  $N_{elim}$ . This arises because we are fitting the simplified model

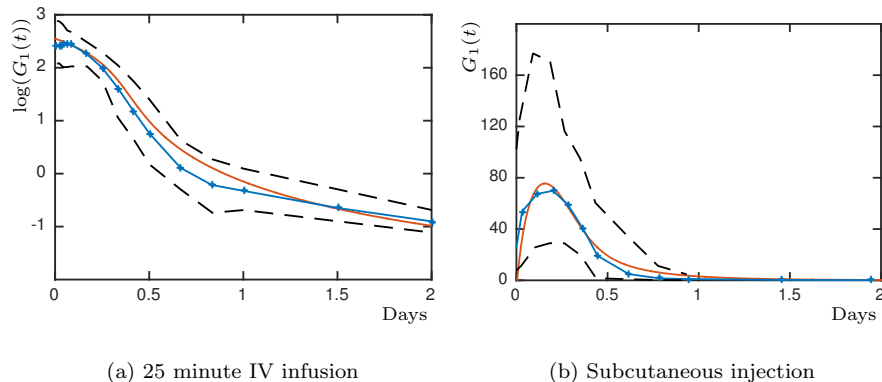


Fig. 5: G-CSF PK parameter fitting results of (68),(69) with parameter values taken from Table 1 with  $N_{elim} = 0.80$ . In both panels, a  $750 \mu\text{g}$  dose is administered following the protocol described in Wang [69]. Blue lines with data: digitised data median values, red solid lines: model solution with estimated parameters, black dashed lines: maximum and minimum values of the digitised data.

(68),(69) without any data for the bound G-CSF concentrations. If the model (68),(69) were linear then parameter identifiability theory would require data from both components of the solution in order to identify unique parameters in the model. Even though (68),(69) is nonlinear, the lack of any bound G-CSF data allows us to fit the unbound G-CSF concentrations with different parameter sets, which will result in different solutions for the unmeasured bound G-CSF concentrations. In Section 4.4 we will see that different G-CSF kinetic parameter sets will result in similar G-CSF responses, but markedly different neutrophil dynamics. The small differences in the reported errors  $Err$  in Table 1 are not sufficient alone to make a definitive judgement of which is the optimal parameter set. In the following sections we will study the response of the full system (1)-(17) not just to exogenous G-CSF but also chemotherapeutic treatment (both alone and with prophylactic exogenous G-CSF) which will lead us to conclude that the PK parameters from Table 1 with  $N_{elim} = 0.80$  produce the best model responses to a variety of scenarios.

As seen in Table 1, the estimates obtained for  $N_{tot}$  are significantly larger than  $[N_R^* + N^*]$ . However as Figure 6(d) shows for a  $750 \mu\text{g}$  dose administered by a 25 minute IV infusion,  $N_{tot}$  is an approximate average for  $[N_R(t) + N(t)]$  over the initial part of the simulation. This, along with the similarity between the results given by (4)-(5) and the full model (as illustrated in Figure 2) gives us confidence not only in the simplified model (68)-(69) for estimating the G-CSF kinetic parameters, but also provides additional confirmation that the marrow reservoir neutrophils  $N_R(t)$  must be included along with the total

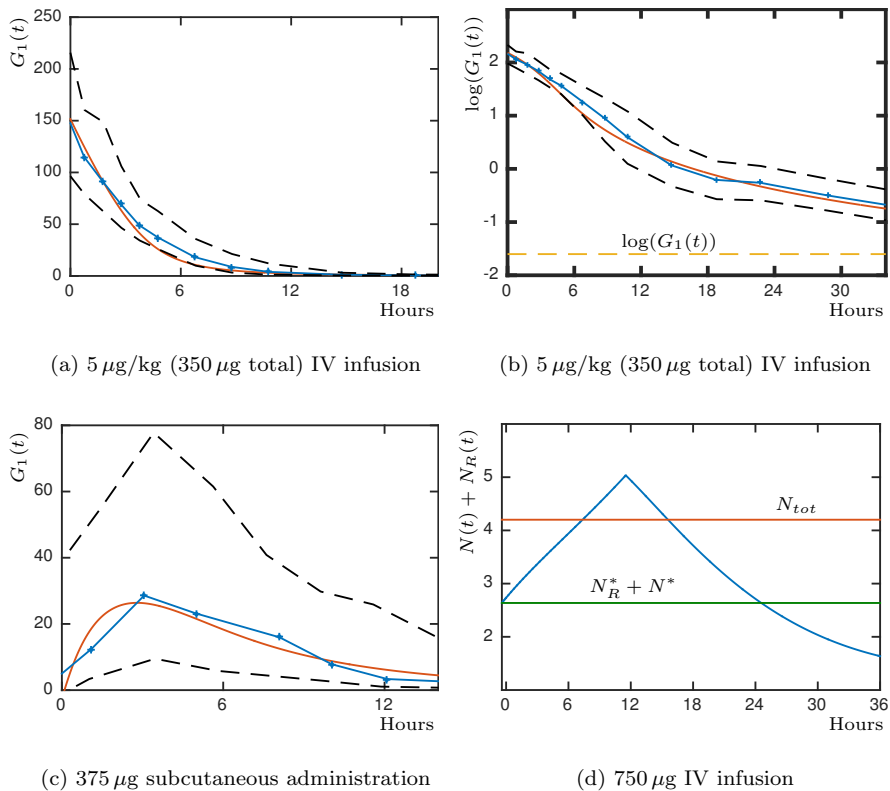


Fig. 6: G-CSF pharmacokinetic parameter fitting results of (68),(69) with parameter values taken from Table 1 with  $N_{elim} = 0.80$  compared for different administration types, doses, and datasets. a) & b) A simulation of (68),(69) is compared to data from [30] in linear and log scales. c) A simulation compared to data from [69]. d) Neutrophil concentrations (blue line) of the full neutrophil model (1)-(17) compared to the value of  $N_{tot}$  and  $N_R^* + N^*$ . For a to c: blue line with data: digitised data median values, red solid line: model solution from estimated parameters, black dashed lines—digitised data maximum and minimum values.

blood neutrophil pool  $N(t)$  in the full kinetic G-CSF model (4)-(5) in order to reproduce the observed physiological response.

#### 4.3 Parameter estimates from G-CSF knockout

Several murine studies [6,34] have looked at the effects of G-CSF knockout by producing mice lacking G-CSF receptors and measuring the differences in circulating neutrophil counts compared to wild type mice. The conclusion of these studies is that even in the case of complete incapacity of the neutrophils

to bind with G-CSF, neutrophil counts were still between 20 and 30% of normal levels. This is consistent with G-CSF not being the sole cytokine to regulate neutrophil production. Consequently we will ensure that our model produces reduced but non-zero circulating neutrophil concentrations in the complete absence of G-CSF, and so in this section we consider the behaviour of the equations defining neutrophil production when  $G_1 \equiv G_2 \equiv 0$ . In that case the four G-CSF dependent functions take values  $\kappa(0) = \kappa^{min}$ ,  $\eta_{NP}(0) = \eta_{NP}^{min}$ ,  $V_{NM}(0) \in (0, 1)$  (by (33)), and  $\varphi_{NR}(0) \in (0, \varphi_{NR}^*)$  (by (31)).

We let  $N_{ko}^*$  denote the total blood neutrophil pool under G-CSF knockout and define the ratio

$$C_{ko} = N_{ko}^*/N^*. \quad (77)$$

Let  $\theta = R_{Pko}/R_P^*$  be the ratio of the rate of cells leaving proliferation in the absence of G-CSF to the rate of cells leaving proliferation at homeostasis. Using (47) and a similar calculation for  $R_{Pko}$  we obtain

$$\theta = \frac{R_{Pko}}{R_P^*} = \frac{\kappa^{min} Q^* e^{\tau_{NP} \eta_{NP}^{min}}}{\kappa^* Q^* e^{\tau_{NP} \eta_{NP}^*}} = \frac{\kappa^{min}}{\kappa^*} e^{\tau_{NP} \eta_{NP}^* (\mu - 1)}, \quad (78)$$

where we also introduce the second auxiliary parameter

$$\mu = \eta_{NP}^{min} / \eta_{NP}^* \leq 1, \quad (79)$$

which measures the fractional reduction in the proliferation rate at knockout. In (78) we have assumed that the number of stem cells is unchanged at knockout. Since the differentiation rate to neutrophils will be decreased from  $\kappa^*$  to  $\kappa^{min}$  in the absence of G-CSF, the number of stem cells will actually increase, but using (44) and (6) this increase can be calculated and is found to be less than 1% for our model parameters.

For given values of  $\theta$ ,  $\mu$  and  $e^{\tau_{NP} \eta_{NP}^*}$  we will use (78) to determine the ratio  $\kappa^{min}/\kappa^*$ . Since  $\kappa^{min} \leq \kappa^*$  (see (32)), (78) implies that  $\theta \leq e^{\tau_{NP} \eta_{NP}^* (\mu - 1)}$ . Rearranging this gives a lower bound for  $\mu$ , from which obtain the constraint

$$\mu \in \left( 1 + \frac{\ln(\theta)}{\tau_{NP} \eta_{NP}^*}, 1 \right). \quad (80)$$

Here  $\mu = 1$  corresponds to a constant proliferation rate independent of G-CSF, with the reduced production of neutrophils at knockout caused by a reduction of the differentiation rate  $\kappa$ . If  $\mu$  is equal to its lower bound then  $\kappa$  is constant independent of G-CSF concentration, and the reduced production of neutrophils is caused by the reduced effective proliferation rate  $\eta_{NP}$ . For intermediate values of  $\mu$ , both  $\kappa^{min}$  and  $\eta_{NP}^{min}$  are reduced from their homeostasis values, and  $\mu$  acts as a tuning parameter to weight the relative contribution of each mechanism with  $\kappa^{min}/\kappa^*$  a monotonically decreasing function of  $\mu = \eta_{NP}^{min} / \eta_{NP}^*$ .

A value for  $\theta$  can be computed by studying the dynamics in the absence of G-CSF after the proliferation stage. Letting  $N_{ko}^*$  and  $N_{Rko}^*$  denote the number of neutrophils at knockout in the total blood pool and in the marrow reservoir



respectively, the rate that cells enter and leave circulation should be equal implying that  $\gamma_N N_{ko}^* = \varphi_{N_R}(0) N_{Rko}^*$ , or

$$N_{Rko}^* = \frac{1}{\varphi_{N_R}(0)} \gamma_N N_{ko}^*. \quad (81)$$

The rate  $R_{Mko}$  that mature neutrophils are created at knockout is then equal to the rate that neutrophils enter and leave the marrow reservoir, and hence

$$R_{Mko} = (\varphi_{N_R}(0) + \gamma_{N_R}) N_{Rko}^* = \gamma_N N_{ko}^* \left( 1 + \frac{\gamma_{N_R}}{\varphi_{N_R}(0)} \right). \quad (82)$$

During G-CSF knockout, the maturation time is given by  $a_{N_M}/V_{N_M}(0)$ , during which cells die at a constant rate  $\gamma_{N_M}$  (which is not affected by G-CSF). Hence the rate  $R_{Pko}$  that cells exit proliferation in the absence of G-CSF is related to  $R_{Mko}$  by

$$R_{Pko} e^{-\gamma_{N_M} \frac{a_{N_M}}{V_{N_M}(0)}} = R_{Mko}.$$

Thus,

$$R_{Pko} = e^{\gamma_{N_M} \frac{a_{N_M}}{V_{N_M}(0)}} R_{Mko} = \gamma_N N_{ko}^* \left( 1 + \frac{\gamma_{N_R}}{\varphi_{N_R}(0)} \right) e^{\gamma_{N_M} \frac{a_{N_M}}{V_{N_M}(0)}}. \quad (83)$$

A similar calculation yields  $R_P^*$ , the rate that cells leave proliferation at homeostasis (with G-CSF), as

$$R_P^* = \gamma_N N^* \left( 1 + \frac{\gamma_{N_R}}{\varphi_{N_R}^*} \right) e^{\gamma_{N_M} a_{N_M}}. \quad (84)$$

Then

$$\theta = \frac{R_{Pko}}{R_P^*} = C_{ko} \frac{\varphi_{N_R}(0) + \gamma_{N_R}}{\varphi_{N_R}^* + \gamma_{N_R}} \exp \left[ a_{N_M} \gamma_{N_M} \left( \frac{1}{V_{N_M}(0)} - 1 \right) \right], \quad (85)$$

where  $C_{ko}$  is defined by (77).

#### 4.4 Estimating the Pharmacodynamic Parameters

We still require estimates for six parameters,  $\mu$ ,  $b_{N_P}$ ,  $V_{max}$ ,  $b_V$ ,  $b_G$  and  $\varphi_{N_R}^{max}$  in the functions defining the pharmacodynamic effects of G-CSF on the neutrophil production and mobilisation.

We digitised data from Wang [69] for average circulating neutrophil concentrations for three days following a 375  $\mu\text{g}$  and a 750  $\mu\text{g}$  25-minute IV infusion. The data also contained circulating G-CSF concentrations, but we did not use the G-CSF concentrations for fitting. As in Section 4.2, instead of fitting directly to the data points we used it to define two continuous functions  $N_{dat}^{375}(t)$  and  $N_{dat}^{750}(t)$ , one for each dose, and fit the response of the full model (1)-(17) to these functions.

The fitting is difficult because no data is available for reservoir or stem cell concentrations, and the circulating neutrophil concentrations are only measured for three days after the infusion. Since the proliferation time for neutrophil precursors is about a week, this data cannot be used to fit any stem cell parameters, as no cells that commit to differentiate to the neutrophil line after the infusion will reach circulation during this time (which is why we do not re-estimate any stem cell parameters in the current work). Although at homeostasis it also takes about a week for cells to traverse maturation and the marrow reservoir, these processes are greatly sped up after G-CSF administration, and cells that are in proliferation at the time of the infusion can reach circulation within a day, enabling us to estimate relevant parameters.

After three days the neutrophil concentrations have not returned to their homeostatic values. If parameters are fit just using this short interval of data, we found parameters which gave good fits to the circulating neutrophil concentrations over the first three days, but for which the neutrophil concentrations then underwent very large deviations from homeostasis values lasting months or more. There is no evidence of a single G-CSF administration destabilising granulopoiesis [39]. Accordingly, we will require that the fit parameters result in stable dynamics. We do this by adding artificial data points for  $7 \leq t \leq 21$  days. Accordingly we construct  $N_{dat}^{375}(t)$  and  $N_{dat}^{750}(t)$  over two disjoint time intervals as splines through the data points for  $t \in [0, 3]$  and as constant functions  $N_{dat}^{dose}(t) = N^*$  for  $t \in [7, 21]$ . Since we have no data for  $t$  between 3 and 7 days describing how the neutrophils return to homeostasis, we do not define values for  $N_{dat}^{dose}(t)$  for this time interval.

For candidate parameter values, we then used Matlab's [38] delay differential equation solver *ddesd* to simulate (1)-(17) over the full 21-day time interval. This defined the functions  $N^{375}(t)$  and  $N^{750}(t)$ , from which we were able to measure the error between the data and the simulated solutions using an  $L^2$  function norm similar to the one defined in (70). For the disjoint time intervals, we have two integrals to perform, and rescale them to carry equal weight and hence define

$$\|N\|_2^2 = \frac{1}{3} \int_0^3 N(t)^2 dt + \frac{1}{14} \int_7^{21} N(t)^2 dt, \quad (86)$$

with corresponding fitting error

$$Err = \|N_{dat}^{375}(t) - N^{375}(t)\|_2^2 + \|N_{dat}^{750}(t) - N^{750}(t)\|_2^2. \quad (87)$$

Parameter estimation was performed using the *fmincon* function in Matlab [38]. As in the G-CSF fitting described in Section 4.2, the error was evaluated by sampling the functions at one thousand points (with 500 in each time interval because of the scaling in (86)).

Instead of directly fitting the six parameters specified at the start of this section, we let  $\tilde{b}_V = b_V/V_{max}$  and fit to the six parameters  $\mu$ ,  $b_{Np}$ ,  $V_{max}$ ,  $\tilde{b}_V$ ,  $\varphi_{N_R}(0)$  and  $\varphi_{N_R}^{ratio}$ . This set of parameters is easier to fit to because the constraints (31) and (33) then become simply  $\varphi_{N_R}(0) > 0$  and  $\tilde{b}_V > G_1^*$ , while

the original constraints both involve more than one of the unknown parameters. From (17),(30) and (78), at each step of the optimisation the six fitting parameters define the remaining parameters via

$$\begin{aligned} \eta_{N_P}^{min} &= \mu \eta_{N_P}^*, & \varphi_{N_R}^{max} &= \varphi_{N_R}^{ratio} \varphi_{N_R}^*, & b_V &= \tilde{b}_V V_{max}, \\ \kappa^{min} &= \theta \kappa^* e^{(\tau_{N_P} \eta_{N_P}^* (1-\mu))}, & b_G &= G_{BF}^* \frac{\varphi_{N_R}^{max} - \varphi_{N_R}(0)}{\varphi_{N_R}^* - \varphi_{N_R}(0)}. \end{aligned} \quad (88)$$

where  $\theta$  itself is calculated from (85). The Hill coefficient of (8) was set to be  $s_1 = 1.5$ , midway within its plausible range of values, as explained in Section 5.

The estimation of  $\mu$  requires some caution as its lower bound in (80) changes at each iteration of the optimisation as  $\theta$  varies, and we see from (85) that  $\theta$  itself depends on three of the parameters to which we are fitting. Nonsensical results are obtained if the model is simulated with  $\mu$  outside its bounds. Since the constraint is difficult to apply, to ensure that (80) is respected we use a penalty method. Consequently, (80) is checked at each iteration of the optimisation and if  $\mu$  is outside of its bounds  $\mu$  is reset to the bound and after the simulation is computed  $Err$  is multiplied by the penalty factor  $e^{|\mu - \mu_{bound}|^{1/2}}$  which is larger than 1 when  $\mu \neq \mu_{bound}$ . The error function thus penalised cannot have a minimum with  $\mu$  outside of its bounds, and so the optimisation routine is forced to find values for  $\mu$  within the permissible range.

A family of G-CSF kinetic parameter sets was reported in Table 1 in Section 4.2. Estimates for the pharmacodynamic parameters were performed for every parameter set in Table 1. The resulting pharmacodynamic parameters are reported in Table 2.

Since  $G_2^*$  in the full model (1)-(17) is given by (66) which differs from the value given by (74) for the simplified model (68),(69), the values of  $G_{prod}$  and  $N_{elim}$  derived for the two models will also be different. In Table 2 the values from Section 4.2 for the simplified model are referred to as  $N_{elim}^{simp}$ , and we also state the corresponding value of  $N_{elim}$  for the full model from (73) using (67).

It is important to note that if  $\mu$  were close to 1 and far from its lower bound, then  $\kappa^{min}/\kappa^* \ll 1$ , and the wide variation in possible differentiation rates could have potentially destabilising effects on the stem cells. However, for most of the investigated parameter sets (except for  $N_{elim}^{simp} = 0.097478$ ) with the added ‘stabilising’ data,  $\mu$  was found to be essentially equal to its lower bound. In this case  $\kappa^{min}$  is almost equal to  $\kappa^*$ , and the rate of differentiation out of the stem cell compartment is essentially constant and (8) is virtually independent of the influence of G-CSF. For the current model with the imposed stabilising data, this implies that any change in production is produced by variations in the effective proliferation rate of (9). Without the additional data points, we found parameter estimates where  $\mu$  was far from its lower bound and  $\kappa^{min}$  was similarly lower than  $\kappa^*$  but these led to unstable dynamics. As seen in Sections 4.5 and 6, the parameter estimates obtained are shown to successfully reproduce protocols for chemotherapy-alone and chemotherapy with adjuvant G-CSF. Accordingly, differentiation from the hematopoietic stem cells is likely

Name	Value 1	Value 2	Value 3	Value 4	Value 5	Units
$N_{elim}^{simp}$	0.097478	0.6	0.71678	0.8	0.87358	—
$N_{elim}$	0.3631	0.4508	0.6204	0.7033	0.8153	—
$\mu$	0.96381	0.86303	0.85482	0.84458	0.90768	—
$b_{NP}$	0.125	0.026182	0.025994	0.022868	0.024908	ng/mL
$V_{max}$	7.9932	7.9881	7.9697	7.867	7.994	—
$\tilde{b}_V$	0.031250	0.031251	0.031255	0.031283	0.031261	ng/mL
$\varphi_{NR}(0)$	0.072801	0.026753	0.023154	0.020056	0.049852	days <sup>-1</sup>
$\varphi_{NR}^{ratio}$	10.9606	11.7257	11.9442	11.3556	11.9706	—
$\eta_{NP}^{min}$	1.6045	1.4367	1.4231	1.406	1.5111	days <sup>-1</sup>
$\varphi_{NR}^{max}$	3.9897	4.2682	4.3478	4.1335	4.3574	days <sup>-1</sup>
$b_V$	0.24979	0.24964	0.24909	0.24611	0.2499	ng/mL
$b_G$	$6.3999 \times 10^{-5}$	0.0002107	0.00019058	0.00018924	0.00018725	—
$\theta$	0.45978	0.18895	0.17099	0.15096	0.32529	—
$\kappa^{min}$	0.0052359	0.0073325	0.0073325	0.0073325	0.0073325	days <sup>-1</sup>
$Err$	0.3482	0.3153	0.2928	0.2843	0.3762	—

Table 2: Parameter estimation results for the pharmacodynamic parameters.  $N_{elim}^{simp}$  refers to  $N_{elim}$  value of the corresponding kinetic parameters for the simplified G-CSF model given in Table 1.  $N_{elim}$  is the corresponding value for the full model, then stated are the six fit parameters, followed by the dependent parameters. The approximation error to the data is found by integrating (3) as in (87) and comparing to Wang’s data [69] for a 375  $\mu\text{g}$  and 750  $\mu\text{g}$  IV infusion of 25 minutes.

close to constant in reality but from our results, we cannot conclude that differentiation is independent of G-CSF.

Figure 7, compares the resulting model solutions for three different values of  $N_{elim}$ , two of which are shown to be less optimal. Also included are the corresponding G-CSF predictions without any re-estimation from the values obtained in Section 4.2. For  $N_{elim} = 0.097478$ , the G-CSF response is well predicted as seen in Figure 7b but because of the renal domination of these parameters, the cytokine paradigm fails in the endogenous-only case. Moreover, repeated administrations of exogenous G-CSF will not accumulate per clinical observations. The G-CSF response seems to be well characterised by the  $N_{elim}^{simp} = 0.87358$  parameters in Figure 7f however the dynamics of the neutrophil response in Figure 7e do not stay within the data bounds, and so are not a good fit. Using  $N_{elim}^{simp} = 0.80$ , both the neutrophil and G-CSF responses are successfully predicted in Figures 7c and 7d. The two sets with the lowest errors ( $N_{elim}^{simp} = 0.71678$  and  $N_{elim}^{simp} = 0.8$ ) were used to determine parameters relating to the pharmacodynamic effects of chemotherapy, which is discussed in Section 4.5.

#### 4.5 Estimation of Chemotherapy Related Parameters

To estimate parameters in (38) and (40), data from the results of the Phase I clinical trial of Zalypsis<sup>®</sup> were digitised from González-Sales [22]. Unlike the

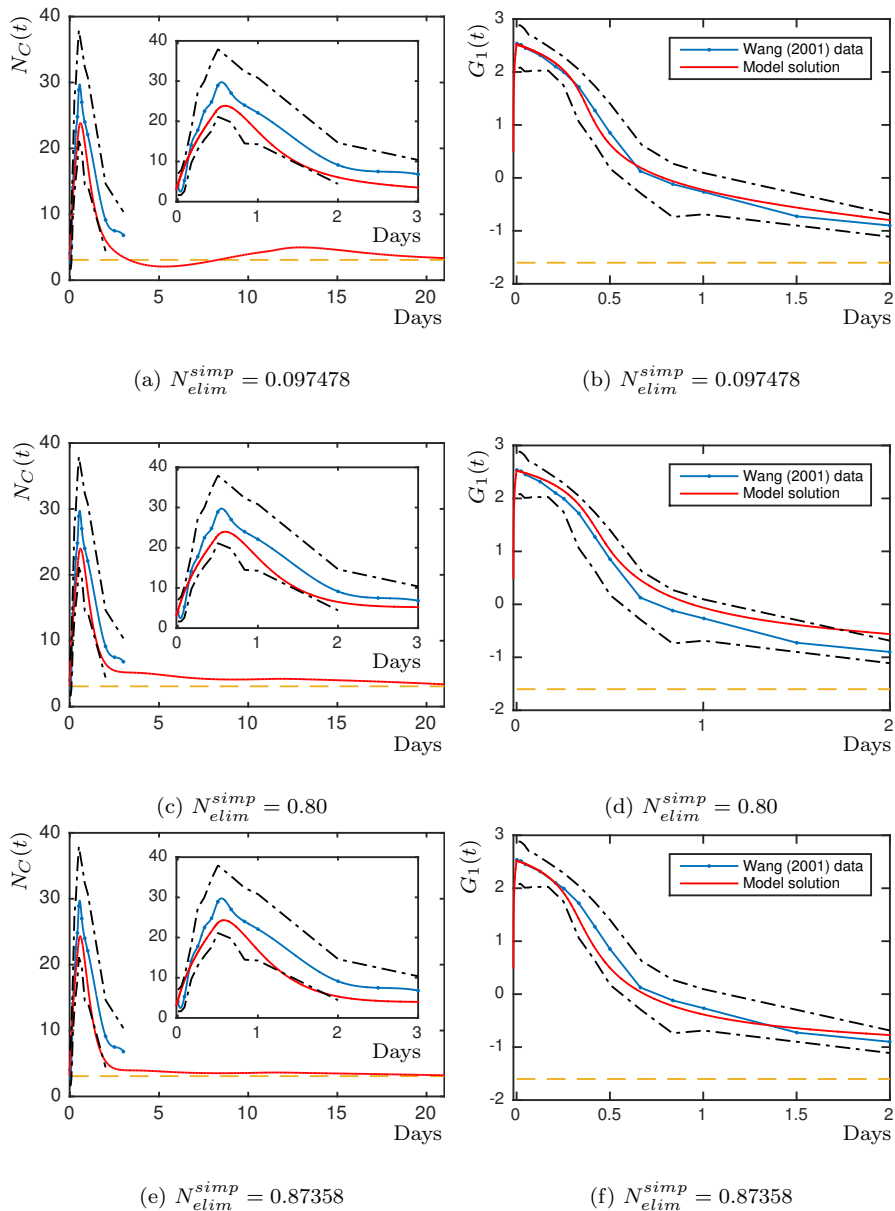


Fig. 7: Simulations of the full model (1)-(17) for various parameter sets with different  $N_{elim}$  values. Left: Circulating neutrophil concentrations in  $10^9$  cells/kg over 21 days, with the first three days shown as an inset. Right: The corresponding circulating G-CSF concentrations. Blue lines with data: digitised data from Figure 7 (neutrophil concentrations) and Figure 6 (G-CSF concentrations) of Wang [69], red solid lines: model solution, black dashed lines: maximum and minimum digitised data values from Figure 7 and Figure 6 of [69], yellow dashed lines: respective homeostatic values.

data used for fitting in Sections 4.2 and 4.4, here the protocols differ from one subject to the next and are reported per patient. All dosing regimens were as stated [22] with doses scaled by body surface area (BSA). Since the subjects were patients undergoing anti-cancer treatments, deviations from the prescribed protocols were frequent. Thus only subjects in the top row (A, B) and bottom row (D, E) of Figure 3 in [22] were retained for our analyses.

As with the parameter estimation of the two previous sections, we define the function  $N_{dat}^{ch_j}(t)$  from a spline fit to the data, where  $j = A, B, D, E$  corresponds to each of the retained subjects. Likewise, the function  $N^{ch_j}(t)$  was defined from the solution from the DDE solver *ddesd* in Matlab [38] for each patient. When the subject was administered two or more cycles of chemotherapy, we took time intervals corresponding to the first two cycles. Thus, the time spans differed for each subject-specific fitting procedure and were:  $t_{span_A} = [0, 43]$ ,  $t_{span_B} = [0, 41]$ ,  $t_{span_C} = [0, 47]$ , and  $t_{span_D} = [0, 61]$ . As explained in Section 5, to account for each subject's baseline ANC, we adjust a scaling factor so our homeostasis  $N^*$  value matches each individual's. We have previously shown the robustness of a similar model to pharmacokinetic interindividual and interoccasion variability which substantiates this adjustment and the use of average values in physiological models [10]. For each of the four patients, we define the integrals

$$\frac{1}{|t_{span_j}|} \int_{\min(t_{span_j})}^{\max(t_{span_j})} N(t)^2 dt, \quad (89)$$

where  $j = A, B, D, E$ . To find average parameter values which fit to all four patients together, we further defined the average error in the  $L^2$  function norm of (70) between the simulated solutions and the data by

$$Err = \frac{1}{4} \sum_j \|N^{ch_j}(t) - N_{dat}^{ch_j}(t)\|_2^2. \quad (90)$$

Name	Value 1	Value 2	Units
$N_{elim}^{simp}$	0.71678	0.8	–
$N_{elim}$	0.6204	0.7033	–
$h_Q$	0.0071122	0.0079657	–
$EC_{50}$	0.78235	0.72545	ng/mL
$s_c$	0.90568	0.89816	–
$\eta_{NP}^{inf}$	0	0	days <sup>-1</sup>
$Err$	0.17068	0.16965	–

Table 3: Results of the parameter estimation of chemotherapy effects values.

Parameters  $h_Q$ ,  $\eta_{NP}^{inf}$ ,  $s_c$ , and  $EC_{50}$  were then estimated using the *lsqcurvefit* optimisation routine in Matlab [38] and similarly averaged. These values

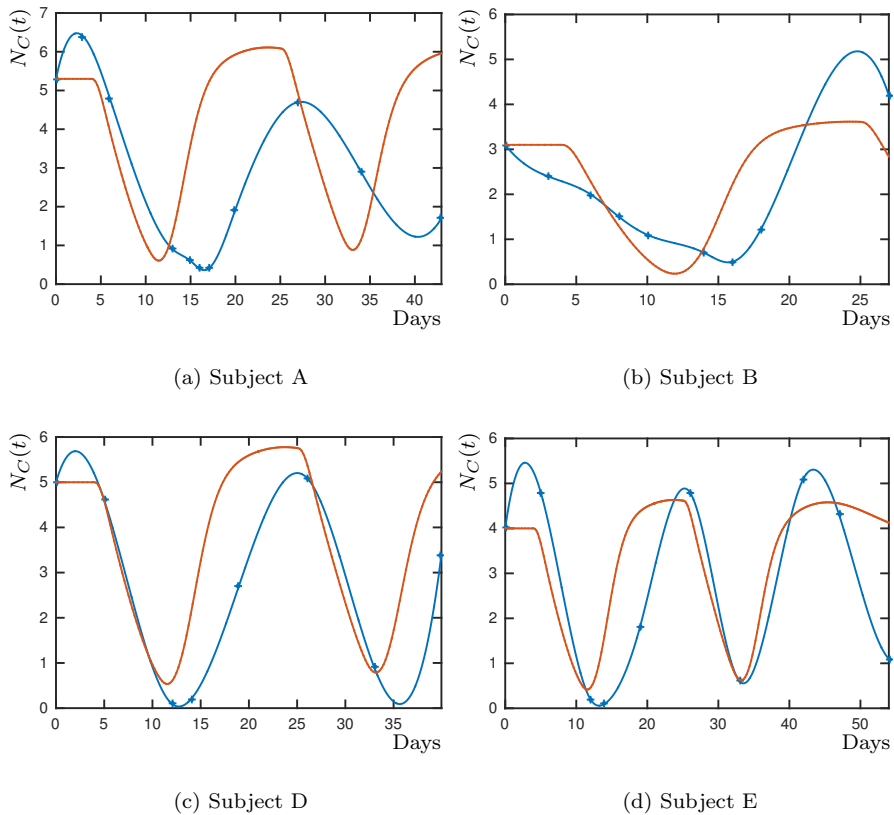


Fig. 8: Results from the chemotherapy parameter fitting for  $N_{elim}^{simp} = 0.80$  parameters over two chemotherapy cycles. Model solutions were obtained using the parameters given in Table 2 and by simulating the full model (1)-(17). Chemotherapeutic concentrations are obtained via (37) and (40). Equation (18) is replaced by (38) and solved by using (39) Data and experimental protocols from Figure 3 of González-Sales [22]. Blue lines with data: digitised data, red solid lines: model solution.

are reported in Table 3 and the results of Figure 8 were obtained from simulations using these parameters. For each of  $h_Q$ ,  $EC_{50}$ ,  $s_c$ , and  $\eta_{N_P}^{inf}$ , similar estimates were obtained for  $N_{elim}^{simp} = 0.71578$  and  $N_{elim}^{simp} = 0.8$ , although the average error of  $N_{elim}^{simp} = 0.8$  is slightly smaller and was accordingly retained as optimal.

## 5 Parameter Values

Here we summarise the parameter values we use in the full model taken from experimental results and the fitting procedures described in Section 4. For the model to be self-consistent these parameters must be positive and satisfy the parameter constraints that we derived above, namely: (30), (31), (33), (59), (60) and (80).

The main model parameters are stated in Table 4. For the stem cells we reuse parameter values for  $Q^*$ ,  $\gamma_Q$ ,  $\tau_Q$ ,  $f_Q$ ,  $s_2$  and  $\beta(Q^*)$  from previous modelling (sometimes rounding them to fewer significant figures). The value of  $\theta_2$  is obtained by evaluating (6) at homeostasis and rearranging to obtain

$$\theta_2 = \left[ \frac{(Q^*)^{s_2} \beta(Q^*)}{f_Q - \beta(Q^*)} \right]^{\frac{1}{s_2}}. \quad (91)$$

In Table 4 we quote a value of  $\theta_2$  to five significant figures, but in our computations all parameters defined by formulae are evaluated to full machine precision. This ensures that our differential equation model has a steady state exactly at the stated homeostasis values.

For the neutrophil parameters we mainly take experimental values from the work of Dancy [14] and use the formulae of Section 4.1 to determine the related model parameter values. However, some choices and adjustments need to be made to ensure that the values are consistent with the model. Dancy [14] measured the circulating neutrophil pool to be  $0.22 \times 10^9$  cells/kg and the recovery rate to be 0.585 from which we obtain the total blood neutrophil pool  $N^*$  (including the marginated pool) to be

$$N^* = \frac{0.22}{0.585} \approx 0.3761 \times 10^9 \text{ cells/kg}. \quad (92)$$

Since  $N(t)$  measures the total blood neutrophil pool in units of  $10^9$  cells/kg some care needs to be taken when comparing to data, where absolute neutrophil counts (ANC) measure the circulating neutrophil pool in units of cell/ $\mu$ L. Based on 70 kg of body mass and 5 litres of blood we have the default conversion factor for healthy subjects of

$$ANC = 0.585 \times \frac{70}{5} \times 1000 \times N(t) = 8190 N(t) \text{ cell}/\mu\text{L}. \quad (93)$$

This gives a baseline homeostasis ANC of  $8190N^* = 3080$  cell/ $\mu$ L, well within the accepted normal range of 1800 – 7000 cells/ $\mu$ L [50]. When comparing our model to data for individuals with different baseline ANCs (as in Section 4.5) we adjust the conversion factor (93), but not the parameter values in our model, so that  $N^*$  gives the homeostasis ANC of the data.

Dancy [14] measures the proliferation and maturation phases at homeostasis to be  $N_P^* = 2.11 \times 10^9$  cells/kg (mainly promyelocytes and myelocytes) and  $N_M^* = 3.33 \times 10^9$  cells/kg (metamyelocytes and bands). Using these numbers in the calculations in Section 4.1 results in a proliferation time  $\tau_{N_P}$  defined



Name	Interpretation	Value	Units	Source
$\gamma_Q$	HSC apoptosis rate	0.1	days <sup>-1</sup>	[5, 11]
$\tau_Q$	Time for HSC re-entry	2.8	days	[35, 4, 33, 11]
$A_Q^*$	HSC Amplification Factor	1.5116 <sup>†</sup>	–	Eq. (7)
$f_Q$	Maximal HSC re-entry rate	8	days <sup>-1</sup>	[4, 5, 11]
$s_2$	HSC re-entry Hill coefficient	2	–	[4, 5, 11]
$\theta_2$	Half-effect HSC concentration	0.080863 <sup>†</sup>	10 <sup>6</sup> cells/kg	Eq. (91)
$\kappa_\delta$	HSC differentiation rate to other lines	0.014665 <sup>†</sup>	days <sup>-1</sup>	Eq. (45)
$\kappa^{min}$	HSC-neutrophil minimal differentiation rate	0.0073325 <sup>†</sup>	days <sup>-1</sup>	Eq. (88)
$\kappa^*$	HSC-neutrophil homeo differentiation rate	0.0073325 <sup>†</sup>	days <sup>-1</sup>	Eq. (45)
$s_1$	HSC-neutrophil differentiation Hill coefficient	1.5	–	Eq. (96)
$\eta_{NP}^*$	Neutrophil homeostasis effective proliferation rate	1.6647 <sup>†</sup>	days <sup>-1</sup>	Eq. (63)
$b_{NP}$	Neutrophil proliferation M-M constant	0.022868	ng/mL	Fit Table 2
$\eta_{NP}^{min}$	Neutrophil minimal proliferation rate	1.4060	days <sup>-1</sup>	Eq. (88)
$\tau_{NP}$	Neutrophil proliferation time	7.3074 <sup>†</sup>	days	Eq. (64)
$V_{max}$	Maximal neutrophil maturation velocity	7.8670	–	Fit Table 2
$b_V$	maturation velocity half-effect concentration	0.24611	ng/mL	Eq. (88)
$a_{NM}$	Homeostasis neutrophil maturation time	3.9	days	[14, 25] & (95)
$\gamma_{NM}$	Neutrophil death rate in maturation	0.15769 <sup>†</sup>	days <sup>-1</sup>	Eq. (57)
$\varphi_{NR}^*$	Homeostasis Reservoir Release rate	0.36400 <sup>†</sup>	days <sup>-1</sup>	Eq. (52)
$\varphi_{NR}^{max}$	Maximal Reservoir Release rate	4.1335 <sup>†</sup>	days <sup>-1</sup>	Eq. (88)
$b_G$	Reservoir Release half-effect concentration	$1.8924 \times 10^{-4}$	–	Eq. (88)
$\gamma_{NR}$	Neutrophil death rate in reservoir	0.0063661 <sup>†</sup>	days <sup>-1</sup>	Eq. (54)
$\gamma_N$	Neutrophil Removal Rate from Circulation	35/16	days <sup>-1</sup>	Eq. (51)
$G_1^*$	Homeostasis Free G-CSF Concentration	0.025	ng/mL	[71, 26, 2, 30]
$G_{BF}^*$	Homeostasis neutrophil receptor bound fraction	$1.5823 \times 10^{-5}$	–	Eq. (16)
$G_{prod}$	Endogenous G-CSF production rate	0.014161 <sup>†</sup>	ng/mL/day	Eq. (67)
$V$	Bound G-CSF conversion factor	0.525	$\frac{\text{ng/mL}}{10^9 \text{ cells/kg}}$	Eq. (65)
$k_{ren}$	G-CSF renal elimination rate	0.16139	days <sup>-1</sup>	Fit Table 1
$k_{int}$	G-CSF effective internalisation rate	462.42	days <sup>-1</sup>	Fit Table 1
$k_{12}$	G-CSF Receptor binding coefficient	2.2423	(ng/mL) <sup>-Pow</sup> days <sup>-1</sup>	Fit Table 1
$k_{21}$	G-CSF Receptor unbinding rate	184.87	days <sup>-1</sup>	Fit Table 1
$Pow$	Effective G-CSF binding coefficient	1.4608	–	Fit Table 1

Table 4: Model Parameters. <sup>†</sup> – these parameters are displayed to 5 significant figures here, but the value is actually defined by the stated equation, and in simulations/computations we use the stated formula to define the value to machine precision.

by (64) of about 26 days. In our model  $\tau_{NP}$  is the time from when the HSC first commits to differentiate to the neutrophil line to the end of proliferation of the neutrophil precursors. Although this time has never been definitively measured, 26 days seems to be too long. This is confirmed by the time to neutrophil replenishment in the blood after both allogenic and autologous stem cell transplantation [1, 7], where circulating neutrophils are seen two weeks after the transplant. We suspect that this overly long proliferation time results from the simplification in our model of considering proliferation as a single homogenous process as detailed in Section 3.3.

To obtain a more realistic proliferation time of around a week, close to the 6.3 days that Smith [62] states, we keep the total of  $N_P^* + N_M^* = 5.44 \times 10^9$  cells/kg as found by Dancy [14], but redistribute cells between pro-

Name	Interpretation	Value	Units	Source
$Q^*$	HSC homeostasis concentration	1.1	$10^9$ cells/kg	[4, 33, 11]
$\beta(Q^*)$	HSC re-entry rate	0.043	days <sup>-1</sup>	[35, 11]
$N^*$	Homeostasis Total Blood Neutrophil Pool	0.22/0.585	$10^9$ cells/kg	Eq. (92)
$N_R^*$	Homeostasis Neutrophil Reservoir Concentration	2.26	$10^9$ cells/kg	[14]
$N_P^*$	Homeostasis Neutrophil Proliferation Concentration	0.93	$10^9$ cells/kg	Eq. (94)
$N_M^*$	Homeostasis Neutrophil Maturation Concentration	4.51	$10^9$ cells/kg	Eq. (94)
$G_2^*$	Homeostasis bound G-CSF concentration	$2.1899 \times 10^{-5}$	ng/mL	Eq. (66)
$\tau_{NR}^*$	Homeostasis Neutrophil mean time in reservoir	2.7	days	[14, 25] & (95)
$\tau_{NC}^*$	Homeostasis Neutrophil mean time in circulation	16/35	days	[14]
$t_{1/2}$	Circulating Neutrophil half-removal time	7.6	hours	[14]
$A_N^*$	Homeostasis neutrophil proliferation+maturation amplification	$1.0378 \times 10^{5\dagger}$	–	Eq. (61)
$b_V$	scaled maturation half-effect concentration	0.031283	ng/mL	Fit Table 2
$\varphi_{NR}^{ratio}$	Ratio of maximal and homeostasis reservoir release rates	11.356	–	Fit Table 2
$\varphi_{NR}(0)$	Minimal reservoir release rate	0.020056	days <sup>-1</sup>	Fit Table 2
$\theta$	Ratio of rate cells leave proliferation at knockout to homeostasis	0.15096	–	Eq. (85)
$C_{ko}$	Knockout total blood neutrophil pool fraction	0.25	–	[6, 34]
$\mu$	Ratio of minimal and homeostasis proliferation rates	0.84458	–	Fit Table 2

Table 5: Auxiliary Parameters which are not in the model in Section 2, but whose values are used to define other parameters. <sup>†</sup> – these parameters are displayed to 5 significant figures here, but the value is actually defined by the stated equation, and in simulations/computations we use the stated formula to define the value to machine precision.

liferation and maturation and set

$$N_P^* = 0.93 \times 10^9 \text{ cells/kg}, \quad N_M^* = 4.51 \times 10^9 \text{ cells/kg}. \quad (94)$$

Dancey [14] measured the half removal time of neutrophils from circulation to be  $t_{1/2} = 7.6$  hrs. Accordingly, using (51) and rounding, we set  $\gamma_N = 35/16 = 2.1875 \text{ days}^{-1}$  and obtain  $\tau_{NC}^*$  as the reciprocal of this. Then equation (58) imposes the constraint that  $a_{NM} < 5.4823 \text{ days}$ . If we set  $a_{NM} = 3.9 \text{ days}$  close to the value of 3.8 days found by Hearn [25], then (60) imposes the constraint that  $\tau_{NR}^* \in (1.9543, 2.7472)$ . Hence we take

$$a_{NM} = 3.9 \text{ days}, \quad \tau_{NR}^* = 2.7 \text{ days}, \quad (95)$$

so that both constraints are satisfied, and  $a_{NM} + \tau_{NR}^* = 6.6 \text{ days}$ , the value given in [14]. The rest of the neutrophil homeostasis parameters are calculated using the formulae of Section 4.1, paying attention in (61) to multiply  $Q^*$  by  $10^{-3}$  to convert it to the same units as  $N_R^*$ .

The G-CSF pharmacokinetic parameters are fit using the simplified G-CSF model (68),(69) as described in Section 4.2. This produces multiple, but equally plausible, parameter sets but as described in subsequent sections not all of these result in good fits to data when we consider the neutrophil response of the full model (1)-(17) to administrations of G-CSF or of chemotherapy. Consequently as stated in Section 4.5, to obtain the best responses of the system to these scenarios we use the fourth set of pharmacokinetic parameters from Table 1 which for the simplified G-CSF model have  $N_{elim}^{simp} = 0.8$  to define

$k_{ren}$ ,  $k_{12}$ ,  $k_{21}$ ,  $k_{int}$  and  $Pow$ , as well as the exogenous G-CSF parameters  $V_d$ ,  $F$ ,  $k_a$  (where the last three are dose dependent). Equations (66), (67) and (73) then define  $G_2^*$ ,  $G_{prod}$  and  $N_{elim} = 0.7033$  for the full model.

At G-CSF knockout, from [6,34] we have  $C_{ko} \in [0.2, 0.3]$ , so it is natural to set  $C_{ko} = 0.25$ .

For the pharmacodynamic parameters, similar to  $Pow$ , arguments could be made for choosing  $s_1 = 1$  or  $s_1 = 2$ , but having fit  $Pow$  and finding it close to 1.5, we will simply set

$$s_1 = 1.5 \tag{96}$$

to reduce the number of parameters that need to be fit by one. The remaining pharmacodynamic parameters  $\mu$ ,  $b_{N_P}$ ,  $V_{max}$ ,  $\tilde{b}_V$ ,  $\varphi_{N_R}(0)$  and  $\varphi_{N_R}^{ratio}$  were then fit as described in Section 4.4, with these parameters defining values of the dependent parameters  $\eta_{N_P}^{min}$ ,  $\varphi_{N_R}^{max}$ ,  $b_V$  and  $b_G$  via (88). From Section 4.3 we also obtain values for  $\theta$  from (85) and  $\kappa^{min}$  from (88). Each set of kinetic parameters from Table 1 defines a different set of pharmacodynamic parameters as reported in Table 2, but as noted already we prefer the parameter set for  $N_{elim}^{simp} = 0.80$  which corresponds to  $N_{elim} = 0.7033$ .

The full set of parameter values for our combined neutrophil and G-CSF model (1)-(17) are given in Table 4, along with their units, interpretation and source. Since some of these parameters are defined by equations involving auxiliary parameters that do not explicitly appear in the full model we state these parameters and their source in Table 5. Parameters related to the pharmacokinetics and pharmacodynamics of both of the exogenous drugs which have not previously been stated are given in Table 6.

## 6 Model evaluation and functional responses

Having estimated the G-CSF pharmacokinetic, homeostasis related, and chemotherapy pharmacodynamic parameters individually as described in Sections 4.2, 4.4, and 4.5, a convincing evaluation of the ability of the model is to successfully predict data obtained during the concurrent administration of both exogenous drugs. For this, as in [11], we simulated the CHOP14 protocol described in [43] and [42] which includes the administration of both chemotherapy and exogenous G-CSF. Although the chemotherapeutic drug modelled in Section 3.5 is not part of the combination therapy of the CHOP14 regimen, the cytotoxic effects of the anticancer drugs are presumed to be similar. To compare to the CHOP14 data published in [29], we simulated a regimen of six cycles of 14-day periodic chemotherapeutic treatment with rhG-CSF treatment beginning four days after the administration of chemotherapy and continuing for ten administrations per cycle. As in [11], the simulated dose of 4  $\mu\text{g}$  of Zalypsis<sup>®</sup> was selected from the optimal regimens identified in [22] and per the CHOP14 protocol outlined in [43,42], ten 300  $\mu\text{g}$  doses of subcutaneous G-CSF were simulated per cycle. The lower dose of 300  $\mu\text{g}$  was selected since we assumed an average weight of 70kg per patient throughout.

Name	Interpretation	Value	Units	Source
Filgrastim				
300 mcg dose				
$V_d$	Volume of distribution	4754.7	mL	Fit Table 1
$F$	Bioavailable fraction	0.64466	–	Fit Table 1
$k_a$	Subcutaneous rate of absorption	8.0236	days <sup>-1</sup>	Fit Table 1
375 mcg dose				
$V_d$	Volume of distribution	2322.9	mL	Fit Table 1
$F$	Bioavailable fraction	0.49964	–	Fit Table 1
$k_a$	Subcutaneous rate of absorption	6.6133	days <sup>-1</sup>	Fit Table 1
750 mcg dose				
$V_d$	Volume of distribution	2178.0	mL	Fit Table 1
$F$	Bioavailable fraction	0.75	–	Fit Table 1
$k_a$	Subcutaneous rate of absorption	5.143	days <sup>-1</sup>	Fit Table 1
Zalypsis <sup>®</sup>				
$k_{fp}$	Rate of exchange from compartment $f$ to $p$	18.222	days <sup>-1</sup>	[41]
$k_{sl_1p}$	Rate of exchange from compartment $sl_1$ to $p$	0.6990	days <sup>-1</sup>	[41]
$k_{pf}$	Rate of exchange from compartment $p$ to $f$	90.2752	days <sup>-1</sup>	[41]
$k_{psl_1}$	Rate of exchange from compartment $p$ to $sl_1$	8.2936	days <sup>-1</sup>	[41]
$k_{elC}$	Rate of elimination	132.0734	days <sup>-1</sup>	[41]
$k_{sl_2f}$	Rate of exchange from compartment $sl_2$ to $f$	62.5607	days <sup>-1</sup>	[41]
$k_{fsl_2}$	Rate of exchange from compartment $f$ to $sl_2$	9.2296	days <sup>-1</sup>	[41]
BSA	Body surface area	1.723	m <sup>2</sup>	[41]
$h_Q$	Effect of chemotherapy on $Q(t)$	0.0079657	–	Fit Table 3
$EC_{50}$	Half-maximal effect of chemotherapy on $\eta_{N_P}$	0.75390	–	Fit Table 3
$s_c$	Chemotherapy effect Hill coefficient	0.89816	–	Fit Table 3
$\eta_{N_P}^{inf}$	Proliferation rate with infinite chemotherapy dose	0	days <sup>-1</sup>	Fit Table 3

Table 6: Exogenous drug administration parameters determined by parameter fitting as explained in Sections 4.2 and 4.5. For Zalypsis<sup>®</sup>,  $p$ : plasma/central compartment,  $f$ : fast-exchange tissues,  $sl_1$ : first slow-exchange tissues,  $sl_2$ : second slow-exchange tissues.

Figure 9 shows the result of the neutrophil response comparison of the model's prediction to the clinical data. Unlike experimental settings where information on the HSCs, the marrow neutrophils, and the bound G-CSF concentrations are unavailable, the model's solutions for  $Q(t)$ ,  $N_R(t)$ , and  $G_2(t)$  are easily obtainable and provide insight into not only the mechanisms responsible for myelosuppression during chemotherapy, but also ways in which this toxicity might be avoided. In Figure 10, the HSCs, neutrophils in the marrow reservoir, and bound and unbound G-CSF are all seen to converge to periodic responses. However, while the reduction in HSC concentrations is minimal (Figure 10a) the neutrophil marrow reservoir is seen in Figure 10b to become severely depleted. This depletion is caused by the delayed effects of the administration of chemotherapy but also the rapid transit of cells from the reservoir into the blood caused by the introduction of exogenous G-CSF four days post-chemotherapy (see Figure 11e below). This in turn prevents ANC recoveries from depressed values, despite the administration of G-CSF. As in [66] and [11], it is likely that delaying the beginning of prophylactic G-CSF

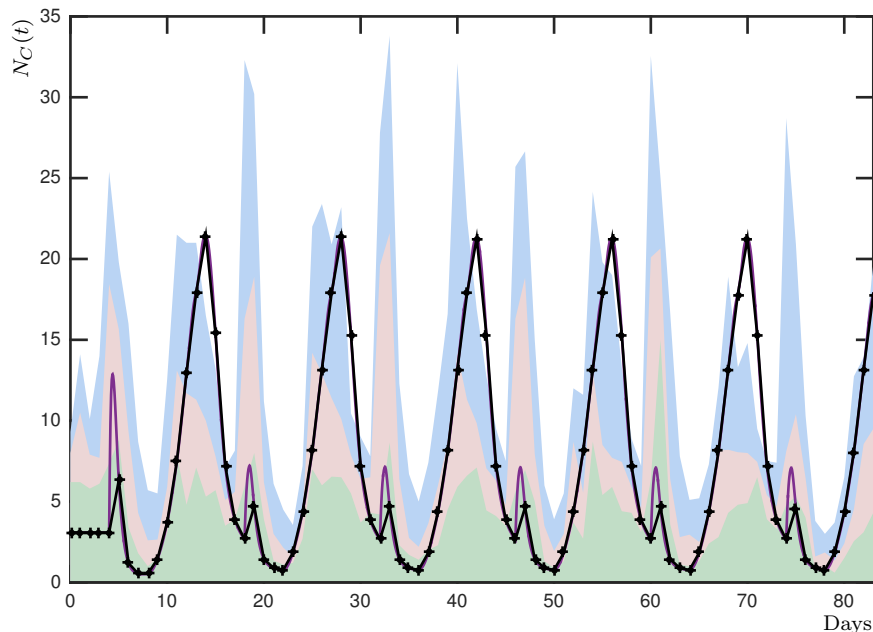


Fig. 9: Comparison of the predicted neutrophil response to the CHOP14 protocol [43, 42] for  $N_{elim}^{simp} = 0.80$ . In this regimen,  $4 \mu\text{g}$  of Zalypsis<sup>®</sup> given by a 1 hour IV infusion is administered 14 days apart, beginning on day 0, for 6 cycles (84 days total). Per cycle, ten administrations of  $300 \mu\text{g}$  subcutaneous doses of filgrastim are given beginning four days after the start of the chemotherapeutic cycle and continuing to day 13 post-chemotherapy. The simulation is compared to data from [29], presented in quartiles. In pale green: the first quartile, in pale pink: median range, in pale blue: third quartile. Black line with sampling points: model prediction sampled every day at clinical sampling points, solid purple line: full model prediction.

support during chemotherapy would help to combat myelosuppression, but this will be a future avenue of investigation.

It can also be illuminating to study how each of the model's functions correspond to the estimated parameters to obtain further insight on the mechanisms of granulopoiesis. Figure 11 shows the functions  $\kappa(G_1)$ ,  $\eta_{N_P}(G_1)$ ,  $\eta_{N_P}^{chemo}(G_1)$ ,  $V_{N_M}(G_1)$ , and  $\varphi_{N_R}(G_{BF})$  and identifies their respective homeostatic levels. We can see that  $\varphi_{N_R}(G_{BF})$  in Figure 11e, has a homeostasis concentration  $\varphi_{N_R}(G_{BF}^*)$  very close to  $\varphi_{N_R}(0)$ . This reflects the ability of the granulopoietic system to respond rapidly in the case of emergencies [47] but also supports the hypothesis that early prophylactic support with G-CSF during chemotherapy may hasten the emptying of the reservoir due to the responsiveness of  $\varphi_{N_R}(G_{BF}(t))$  in particular.

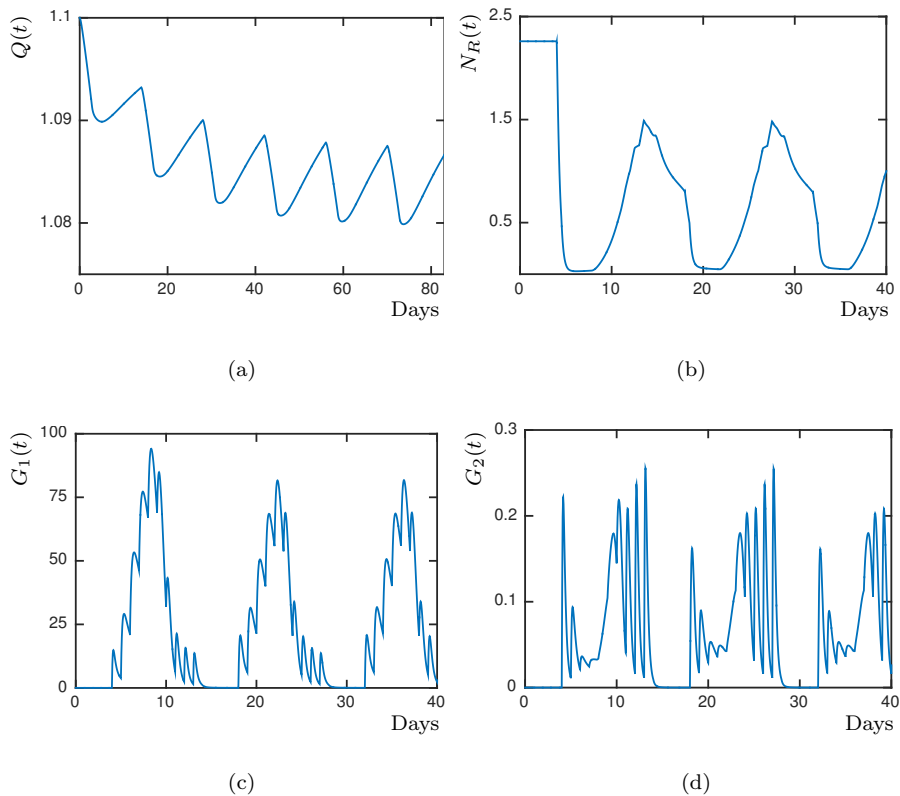


Fig. 10: Model responses to the CHOP14 protocol as described in Section 6. In a)  $Q(t)$  over the six CHOP cycles detailed above, b), c), and d)  $N_R(t)$ ,  $G_1(t)$ , and  $G_2(t)$  over three CHOP cycles.

## 7 Discussion

Clinically relevant translational models in medicine must not only accurately depict different and independent treatment regimes [66], they must also be able to reconstruct homeostatic and pathological cases which may be interventionally independent. The granulopoiesis model we have developed is physiologically-relevant and, perhaps most importantly, provides insight beyond that which is clinically measurable. The updated pharmacokinetic model of G-CSF, novel in that it explicitly accounts for unbound and bound concentrations, correctly accounts for G-CSF dynamics whereas previous one compartment models all resulted in renal dominated dynamics. The new pharmacokinetic model also further allows us to comment on the principle mechanisms driving the production of neutrophils. Although the relatively small number of neutrophil progenitors do not have a significant effect on G-CSF kinetics, our results suggest that differentiation, proliferation and maturation speed are driven primarily by signalling from G-CSF bound to neutrophil progenitors, and not from sig-

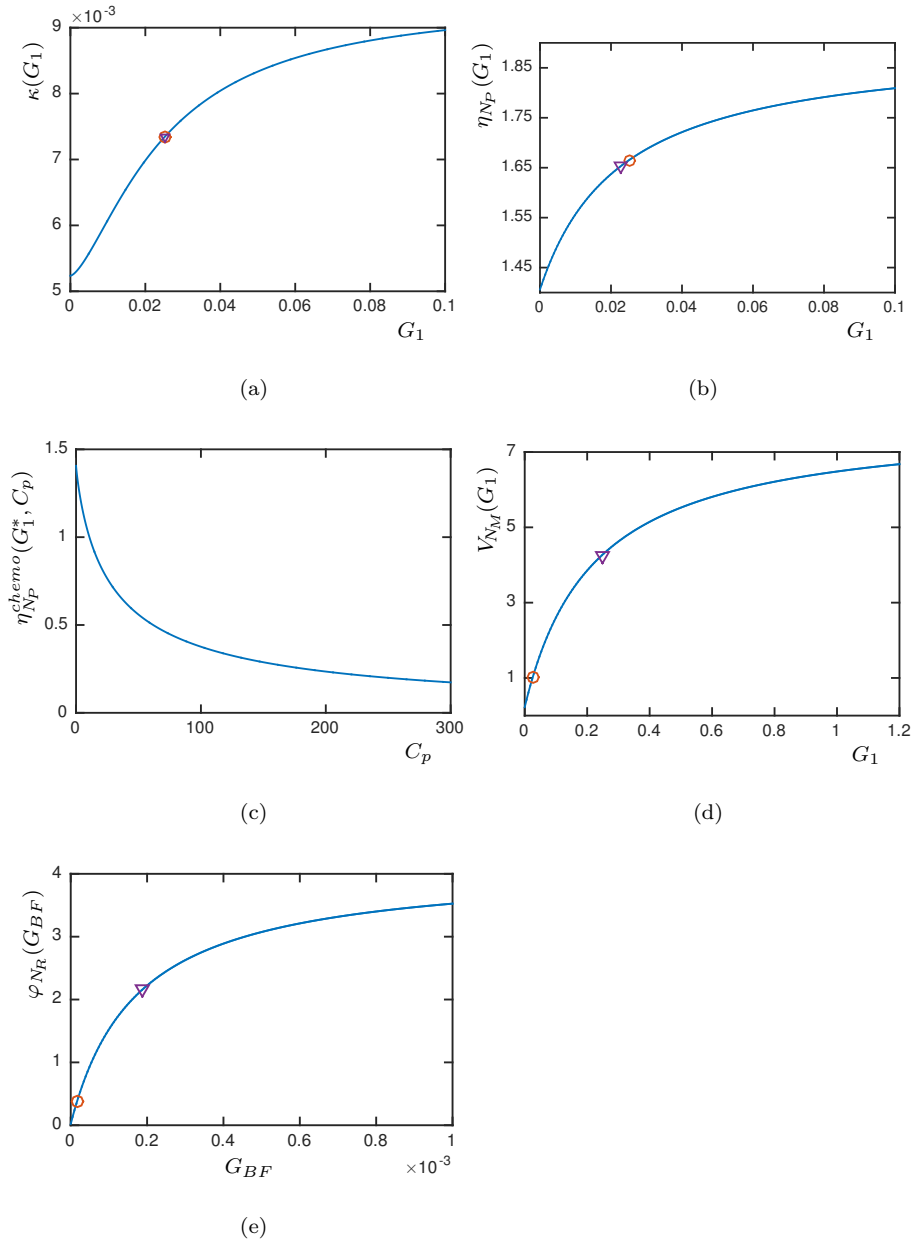


Fig. 11: Visualisation of the granulopoiesis model's mechanisms as functions of their variables (solid blue lines) with their respective homeostatic and half-effect values (purple triangles), when relevant. Red circles: homeostasis values.

nalling of G-CSF bound to mature neutrophils. We can further characterise the

principle processes governing myelosuppression during the concurrent administration of chemotherapy and prophylactic G-CSF, which we have determined lies in the simultaneous depletion of the marrow reservoir by high doses of exogenous G-CSF combined with fewer neutrophils reaching the reservoir due to the cytotoxicity of the anti-cancer drug.

The modelling reported here combines a number of original approaches to the conceptualisation of physiological, pharmacokinetic, and pharmacodynamics models and to the estimation of parameters and model verification. For example, traditional least squares estimation was redefined using functions which ensured robustness and allowed for comparisons of predictions to data over richly sampled intervals instead of at fewer data points. Moreover, the model's physiological realism served as a means of evaluating the suitability of optimised parameter values so we were not relying solely on goodness-of-fit, which can obfuscate the biological relevance of results [67]. The inclusion of the detailed characterisations of physiological mechanisms in our model therefore serves as a litmus test of suitability in addition to providing intuition about the processes driving granulopoiesis.

The broader implications of the approaches outlined in this work extend into various domains. The derivation of a delay differential equation model with variable aging rate from an age-structured PDE, as described in Section 3.3, is mathematically significant and its intricate nature has previously led to previous modelling errors. As mentioned, the fitting procedures outlined in Sections 4.2, 4.4, and 4.5 motivate the development of more refined least squares methods and parameter estimation techniques. Additionally, the novel pharmacokinetic model of G-CSF has ramifications with respect to the usual approaches used by PK/PD modellers. The mischaracterisation of the elimination dynamics, despite the inclusion of internalisation terms, has led to models which contradict what is known of the physiology. While they can characterise certain clinical situations, like the single administration of exogenous G-CSF, they fail when applied to more complex scenarios. Without accounting for the entire process of neutrophil development or using physiological rationale for a model's parameters, one is unable to judge whether a model captures the complicated dynamics of granulopoiesis. In the model we have developed, we have ensured the accuracy of its predictions and the appropriateness of its parameters through careful construction. In turn, this rational approach has implications for the clinical practice where it can serve to optimise dosing regimens in oncological settings and also serve to pinpoint the origins of dynamical neutrophil disorders like cyclic neutropenia, ultimately contributing to the improvement of patient care and outcomes.

## Acknowledgements

ARH and MCM are grateful to the National Science and Engineering Research Council (NSERC), Canada for funding through the Discovery Grant program. MC wishes to thank NSERC for funding from the PGS-D program. We are



grateful to Fahima Nekka, Jun Li, Jacques Bélair, and David Dale for their insight and support.

## References

1. G. Baiocchi, G. Scambia, P. Benedetti, G. Menichella, U. Testa, L. Pierelli, R. Martucci, M.L. Foddai, B. Bizzi, S. Mancuso, and C. Peschle. Autologous stem cell transplantation: Sequential production of hematopoietic cytokines underlying granulocyte recovery. *Cancer Research*, 53:1297–1303, 1993.
2. Daniel R Barreda, Patrick C Hanington, and Miodrag Belosevic. Regulation of myeloid development and function by colony stimulating factors. *Developmental and Comparative Immunology*, 28(5):509 – 554, 2004.
3. S. Basu, G. Hodgson, M. Katz, and A.R. Dunn. Evaluation of role of G-CSF in the production, survival, and release of neutrophils from bone marrow into circulation. *Blood*, 100:854–861, 2002.
4. S. Bernard, J. Bélair, and M.C. Mackey. Oscillations in cyclical neutropenia: New evidence based on mathematical modeling. *Journal of Theoretical Biology*, 223:283–298, 2003.
5. G. Brooks, G.P. Langlois, J. Lei, and M.C. Mackey. Neutrophil dynamics after chemotherapy and G-CSF: The role of pharmacokinetics in shaping the response. *Journal of Theoretical Biology*, 315:97–109, 2012.
6. S. Bugl, S. Wirths, M.R. Müller, and M.P. Radsak. Current insights into neutrophil homeostasis. *Annals of the New York Academy of Sciences: Hematopoietic Stem Cells VIII*, 1266:171–178, 2012.
7. M.S. Cairo, Y. Suen, L. Sender, E.R. Gillan, W. Ho, J.M. Plunkett, and C. van de Ven. Circulating granulocyte colony-stimulating factor (G-CSF) levels after allogeneic and autologous bone marrow transplantation: Endogenous G-CSF production correlates with myeloid engraftment. *Blood*, 79:1869–1873, 1992.
8. C. Colijn and M.C. Mackey. A mathematical model of hematopoiesis: I. Periodic chronic myelogenous leukemia. *Journal of Theoretical Biology*, 237:117–132, 2005.
9. C. Colijn and M.C. Mackey. A mathematical model of hematopoiesis: II. Cyclical neutropenia. *Journal of Theoretical Biology*, 237:133–146, 2005.
10. M. Craig, M. González-Sales, J. Li, and F. Nekka. Impact of pharmacokinetic variability on a mechanistic physiological pharmacokinetic/pharmacodynamic model: A case study of neutrophil development, PM00104, and filgrastim. In B. Toni, editor, *Interdisciplinary Mathematical Research and Applications*. Springer, New York, 2015 (to appear).
11. M. Craig, A.R. Humphries, J. Bélair, J. Li, F. Nekka, and M.C. Mackey. Neutrophil dynamics during concurrent chemotherapy and G-CSF administration: Mathematical modelling guides dose optimisation to minimise neutropenia. *Journal of Theoretical Biology*, 385:77–89, 2015.
12. D.C. Dale and M.C. Mackey. Understanding, treating and avoiding hematological disease: Better medicine through mathematics? *Bulletin of Mathematical Biology*, 77:739–757, 2015.
13. D.C. Dale and K. Welte. *Hematopoietic Growth Factors in Oncology*. Springer, Heidelberg, Germany, 2011.
14. J.T. Dancy, K.A. Deubelbeiss, L.A. Harker, and C.A. Finch. Neutrophil kinetics in man. *The Journal of Clinical Investigation*, 58:705–715, 1976.
15. J.T. DiPiro, W.J. Spruill, W.E. Wade, R.A. Blouin, and J.M. Pruemmer, editors. *Concepts in Clinical Pharmacokinetics*, volume 5. American Society of Health-System Pharmacists, Bethesda, MA, 2010.
16. C. Durand and P. Charbord. *Stem Cell Biology and Regenerative Medicine*, volume 3. River Publishers, Aalborg, Denmark, 2010.
17. M. Ende, M. Etzrodt, and T. Schroeder. Instruction of hematopoietic lineage choice by cytokine signaling. *Experimental Cell Research*, 329:207–213, 2014.

18. C. Foley, S. Bernard, and M.C. Mackey. Cost-effective G-CSF therapy strategies for cyclical neutropenia: Mathematical modelling based hypotheses. *Journal of Theoretical Biology*, 238:756–763, 2006.
19. C. Foley and M.C. Mackey. Dynamic hematological disease: Review. *Journal of Mathematical Biology*, 58:285–322, 2009.
20. C. Foley and M.C. Mackey. Mathematical model for G-CSF administration after chemotherapy. *Journal of Theoretical Biology*, 257:27–44, 2009.
21. L.E. Friberg and M.O. Karlsson. Mechanistic models for myelosuppression. *Investigational New Drugs*, 21:183–194, 2003.
22. M. González-Sales, B. Valenzuela, C. Pérez-Ruixo, C. Fernández Teruel, B. Miguel-Lillo, Soto Matos A., et al. Population pharmacokinetic-pharmacodynamic analysis of neutropenia in cancer patients receiving PM00104 (Zalypsis®). *Clinical Pharmacokinetics*, 51:751–764, 2012.
23. A.M. Greenbaum and D.C. Link. Mechanisms of G-CSF-mediated hematopoietic stem and progenitor mobilization. *Leukemia*, 25:211–217, 2011.
24. W.P. Hammond, E. Csiba, A. Canin, H. Hockman, L.M. Souza, J.E. Layton, and D.C. Dale. Chronic neutropenia. A new canine model induced by human granulocyte colony-stimulating factor. *Journal of Clinical Investigation*, 87:704–710, 2 1991.
25. T. Hearn, C. Haurie, and M.C. Mackey. Cyclical neutropenia and the peripheral control of white blood cell production. *Journal of Theoretical Biology*, 192:167–181, 1998.
26. M Kawakami, H Tsutsumi, T Kumakawa, H Abe, M Hirai, S Kurosawa, M Mori, and M Fukushima. Levels of serum granulocyte colony-stimulating factor in patients with infections. *Blood*, 76(10):1962–1964, 1990.
27. N. D. Kazarinoff and P. van den Driessche. Control of oscillations in hematopoiesis. *Science*, **203**:1348–1350, 1979.
28. E. A. King-Smith and A. Morley. Computer simulation of granulopoiesis: Normal and impaired granulopoiesis. *Blood*, **36**:254–262, 1970.
29. A. Krinner, I. Roeder, M. Loeffler, and M. Scholz. Merging concepts - coupling an agent-based model of hematopoietic stem cells with an ODE model of granulopoiesis. *BMC Systems Biology*, 7:117, 2013.
30. W. Krzyzanski, P. Wiczling, P. Lowe, E. Pigeolet, M. Fink, A. Berghout, and S. Balser. Population modeling of filgrastim PK-PD in healthy adults following intravenous and subcutaneous administrations. *Journal of Clinical Pharmacology*, 9 Suppl:101S–112S, 2010.
31. T. Kuwabara, Y. Kato, S. Kobayashi, H. Suzuki, and Y. Sugiyama. Nonlinear pharmacokinetics of a recombinant human granulocyte colony-stimulating factor derivative (Nartograstim): Species differences among rats, monkeys and humans. *Journal of Pharmacology and Experimental Therapeutics*, 271:1535–1543, 1994.
32. J.E. Layton and N.E. Hall. The interaction of G-CSF with its receptor. *Frontiers in Bioscience*, 31:177–199, 2006.
33. J. Lei and M.C. Mackey. Multistability in an age-structured model of hematopoiesis: Cyclical neutropenia. *Journal of Theoretical Biology*, 270:143–153, 2011.
34. G. Lui, H. Yang, X. Wang, and Y. Chu. Modulation of neutrophil development and homeostasis. *Current Molecular Medicine*, 13:1270–1283, 2013.
35. M.C. Mackey. Cell kinetic status of hematopoietic stem cells. *Cell Proliferation*, 34:71–83, 2001.
36. M.C. Mackey, A.A.G. Aprikyan, and D.C. Dale. The rate of apoptosis in post mitotic neutrophil precursors of normal and neutropenic humans. *Cell Proliferation*, 36:27–34, 2003.
37. V. Maholtra and M.C. Perry. Models of anti-cancer therapy. Classical chemotherapy: mechanism, toxicities, and the therapeutic window. *Cancer Biology and Therapy*, 2:S2–S4, 2003.
38. Mathworks. *MATLAB 2015a*. Mathworks, Natick, Massachusetts, 2015.
39. G.. Molineux. Granulocyte colony-stimulating factors. In G.H. Lyman and D.C. Dale, editors, *Hematopoietic Growth Factors in Oncology*. Springer, 2011.
40. G. Molineux, T. Arvedson, and M. Foote. *Twenty Years of G-CSF Clinical and Non-clinical Discoveries*. Springer Basel AG, Basel, Switzerland, 2012.

41. C. Pérez-Ruixo, B. Valenzuela, C. Fernández Teruel, M. González-Sales, B. Miguel-Lillo, A. Soto-Matos, et al. Population pharmacokinetics of PM00104 (Zalypsis<sup>®</sup>) in cancer patients. *Cancer Chemotherapy and Pharmacology*, 69:15–24, 2012.
42. M. Pfreundschuh, L. Trümper, M. Kloess, R. Schmits, A.C. Feller, C. Rudolph, et al. Two-weekly or 3-weekly chop chemotherapy with or without etoposide for the treatment of elderly patients with aggressive lymphomas: Results of the NHL-B2 trial of the DSHNHL. *Blood*, 104:634–641, 2004.
43. M. Pfreundschuh, L. Trümper, M. Kloess, R. Schmits, A.C. Feller, C. Rudolph, et al. Two-weekly or 3-weekly chop chemotherapy with or without etoposide for the treatment of young patients with good prognosis (normal LDH) aggressive lymphomas: Results of the NHL-B1 trial of the DSHNHL. *Blood*, 104:626–633, 2004.
44. T.H. Price, G.S. Chatta, and D.C. Dale. Effect of recombinant granulocyte colony-stimulating factor on neutrophil kinetics in normal young and elderly humans. *Blood*, 88:335–340, 1996.
45. L. Pujó-Menjouet, S. Bernard, and M.C. Mackey. Long period oscillations in a  $G_0$  model of hematopoietic stem cells. *SIAM Journal of Applied Dynamical Systems*, 4:312–332, 2005.
46. A.L. Quartino, L.E. Friberg, and M.O. Karlsson. A simultaneous analysis of the time-course of leukocytes and neutrophils following docetaxel administration using a semi-mechanistic myelosuppression model. *Investigational New Drugs*, 30:833–845, 2012.
47. S.M. Rankin. The bone marrow: A site of neutrophil clearance. *Journal of Leukocyte Biology*, 88:241–251, 2010.
48. C. Riether, C.M. Schürch, and A.F. Ochsenbein. Regulation of hematopoietic and leukemic stem cells by the immune system. *Cell Death and Differentiation*, 22:187–198, 2015.
49. S. Rubinow and J. Lebowitz. A mathematical model of neutrophil production and control in normal man. *Journal of Mathematical Biology*, 1:187–225, 1975.
50. D.H. Ryan. Examination of blood cells. In K. Kaushansky, M.A. Lichtman, J.T. Prchal, M.M. Levi, O.W. Press, L.J. Burns, and M. Caligiuri, editors, *Williams Hematology*, volume 9. McGraw-Hill Companies, Inc., 2016.
51. M. Santillán. On the use of the Hill functions in mathematical models of gene regulatory networks. *Mathematical Modelling of Natural Phenomena*, 3:85–97, 2008.
52. C.A. Sarkar, K. Lowenhaupt, P.J. Wang, T. Horan, and D.A. Lauffenburger. Parsing the effects of binding, signaling, and trafficking on the mitogenic potencies of granulocyte colony-stimulating factor analogues. *Biotechnology Progress*, 19:955–964, 2003.
53. S. Schirm, C. Engel, M. Loeffler, and M. Scholz. Modelling chemotherapy effects on granulopoiesis. *British Journal of Haematology*, 95:616–625, 1996.
54. S. Schmitz. *Ein mathematisches Modell der zyklischen Haemopoese*. PhD thesis, Universität Köln, 1988.
55. S. Schmitz, H. Franke, M. Loeffler, H.E. Wichmann, and V. Diehl. Model analysis of the contrasting effects of GM-CSF and G-CSF treatment on peripheral blood neutrophils observed in three patients with childhood-onset cyclic neutropenia. *BMC Systems Biology*, 8:1–18, 2014.
56. S. Schmitz, M. Loeffler, J. B. Jones, R. D. Lange, and H. E. Wichmann. Synchrony of bone marrow proliferation and maturation as the origin of cyclic haemopoiesis. *Cell Tissue Kinetics*, 23:425–441, 1990.
57. M. Scholz, C. Engel, and M. Loeffler. Modelling human granulopoiesis under polychemotherapy with G-CSF support. *Journal of Mathematical Biology*, 50:397–439, 2005.
58. M. Scholz, S. Schirm, M. Wetzler, C. Engel, and M. Loeffler. Pharmacokinetic and dynamic modelling of G-CSF derivatives in humans. *Theoretical Biology and Medical Modelling*, 9:1497–1502, 2012.
59. C.L. Semerad, F. Liu, A.D. Gregory, K. Stumpf, and D.C. Link. G-CSF is an essential regulator of neutrophil trafficking from the bone marrow to the blood. *Immunity*, 17:413–423, 2002.
60. E. Shochat, V. Rom-Kedar, and L.A. Segel. G-CSF control of neutrophils dynamics in the blood. *Bulletin of Mathematical Biology*, 69:2299–2338, 2007.
61. D. Shvitra, R. Laugalys, and Y. S. Kolesov. Mathematical modeling of the production of white blood cells. In G. Marchuk and L.N. Belykh, editors, *Mathematical Modeling in Immunology and Medicine*, pages 211–223, Amsterdam, 1983. North-Holland.

62. C.W. Smith. Production, distribution, and fate of neutrophils. In K. Kaushansky, M.A. Lichtman, J.T. Prchal, M.M. Levi, O.W. Press, L.J. Burns, and M. Caligiuri, editors, *Williams Hematology*, volume 9. McGraw-Hill Companies, Inc., 2016.
63. K. Spiekermann, J. Roesler, A. Emmendoerffer, J. Elsner, and K. Welte. Functional features of neutrophils induced by G-CSF and GM-CSF treatment: Differential effects and clinical implications. *Leukemia*, 11:466–478, 1997.
64. K. Terashi, M. Oka, S. Ohdo, T. Furukubo, C. Ikeda, M. Fukuda, H. Soda, S. Higuchi, and S. Kohno. Close association between clearance of recombinant human granulocyte colony-stimulating factor (G-CSF) and G-CSF receptor on neutrophils in cancer patients. *Antimicrobial Agents and Chemotherapy*, 43:21–24, 1999.
65. O. Vainas, S. Ariad, O. Amir, W. Mermershtain, V. Vainstein, M. Kleiman, O. Inbar, R. Ben-Av, A. Mukherjee, S. Chan, and Z. Agur. Personalising docetaxel and G-CSF schedules in cancer patients by a clinically validated computational model. *British Journal of Cancer*, 107:814822, 2012.
66. V. Vainstein, Y. Ginosar, M. Shoham, D.O. Ranmar, A. Ianovski, and Z. Agur. The complex effect of granulocyte colony-stimulating factor on human granulopoiesis analyzed by a new physiologically-based mathematical model. *Journal of Theoretical Biology*, 235:311–327, 2005.
67. P. van der Graaf and N. Benson. Systems pharmacology: Bridging systems biology and pharmacokinetics-pharmacodynamics (PKPD) in drug discovery and development. *Pharmaceutical Research*, 28:1460–1464, 2011.
68. G. K. von Schulthess and N. A. Mazer. Cyclic neutropenia (CN): A clue to the control of granulopoiesis. *Blood*, 59:27–37, 1982.
69. B. Wang, T.M. Ludden, E.N. Cheung, G.G. Schwab, and L.K. Roskos. Population pharmacokinetic-pharmacodynamic modeling of filgrastim (r-metHuG-CSF) in healthy volunteers. *Journal of Pharmacokinetics and Pharmacodynamics*, 28:321–342, 2001.
70. A.C. Ward, J.L. Monkhouse, X.F. Csar, I.P. Touw, and P.B. Bello. The Src-like tyrosine kinase Hck is activated by granulocyte colony-stimulating factor (G-CSF) and docks to the activated G-CSF receptor. *Biochemical and Biophysical Research Communications*, 251(1):117–123, 1998.
71. K. Watari, S. Asano, N. Shirafuji, H. Kodo, K. Ozawa, F. Takaku, and S. Kamachi. Serum granulocyte colony-stimulating factor levels in healthy volunteers and patients with various disorders as estimated by enzyme immunoassay. *Blood*, 73(1):117–122, 1989.
72. H.E. Wichmann and M. Loffler. *Mathematical Modeling of Cell Proliferation: Stem Cell Regulation in Hemopoiesis*. CRC Press, Boca Raton, 1988.
73. X. Wu, F. Nekka, and J. Li. Steady-state volume of distribution of some two compartmental models with immediate linear and saturated eliminations, Under review.